Translational Oncology 45 (2024) 101958

Contents lists available at ScienceDirect

Translational Oncology

journal homepage: www.elsevier.com/locate/tranon

Original Research

20-hydroxyecdysone suppresses bladder cancer progression via inhibiting USP21: A mechanism associated with deubiquitination and degradation of p65

Qiang Ma [a,b,c,d,1], Fei Wu [a,1], Xiaohui Liu [a,1], Cuifang Zhao [a], Yang Sun [c], Yuanyuan Li [c], Wei Zhang [a,c], Hongge Ju [a,c,**], Yukun Wang [b,d,*]

[a] School of Basic and Forensic Medicine, Baotou Medical College, Baotou, China
[b] School of Medicine, Southern University of Science and Technology, Shenzhen, China
[c] Department of Pathology, The First Affiliated Hospital of Baotou Medical College, Baotou, China
[d] Department of Pharmacy, Southern University of Science and Technology Hospital, Shenzhen, China

ARTICLE INFO

Keywords:
Bladder cancer
20-Hydroxyecdysone (20-HE)
USP21
NF-κB/p65

ABSTRACT

Bladder cancer is one of the most common malignancies of the urinary tract and a prevalent cancer worldwide, still requiring efficient therapeutic agents and approaches. 20-Hydroxyecdysone (20-HE), a steroid hormone, can be found in insects and few plants and mediate numerous biological events to control the progression of varying diseases; however, its impacts on bladder cancer remain unclear. In the study, we found that 20-HE treatments effectively inhibited the viability and proliferation of bladder cancer cells and induced apoptosis by activating Caspase-3. The migratory and invasive potential of bladder cancer cells was markedly repressed by 20-HE in a dose-dependent manner. The inhibitory effects of 20-HE on bladder cancer were confirmed in an established xenograft mouse model, as indicated by the markedly reduced tumor growth rates and limited lung and lymph node metastasis. High-throughput RNA sequencing was performed to explore dysregulated genes in bladder cancer cells after 20-HE treatment. We identified ubiquitin-specific protease 21 (USP21) as a key deubiquitinating enzyme for bladder cancer progression and a positive correlation between USP21 and nuclear factor-κB (NF-κB)/p65 in patients. Furthermore, 20-HE treatments markedly reduced USP21 expression, NF-κB/p65 mRNA, stability and phosphorylated NF-κB/p65 expression levels in bladder cancer cells, which were validated in animal tumor tissues. Mechanistic studies showed that USP21 directly interacted with and stabilized p65 by deubiquitinating its K48-linked polyubiquitination in bladder cancer cells, which could be abolished by 20-HE treatment, contributing to p65 degradation. Finally, we found that USP21 overexpression could not only facilitate the proliferation, migration, and invasion of bladder cancer cells, but also significantly eliminated the suppressive effects of 20-HE on bladder cancer. Notably, 20-HE could still perform its anti-tumor role in bladder cancer when USP21 was knocked down with decreased NF-κB/p65 expression and activation, revealing that USP21 suppression might not be the only way for 20-HE during bladder cancer treatment. Collectively, all our results clearly demonstrated that 20-HE may function as a promising therapeutic strategy for bladder cancer treatment mainly through reducing USP21/p65 signaling expression.

Introduction

Bladder cancer is one of the most common cancers worldwide, and its incidence is steadily rising with over 430,000 cases diagnosed each year [1]. Approximately 75 % of patients present with non-muscle-invasive disease (NMIBC), and 70 % of these tumors will recur, while 15 % will progress in stage and grade [2]. Surgical operation and chemotherapy are two main approaches for the treatment of bladder cancer [3]. Over the years, some novel and high accuracy noninvasive assays have been developed to search genetic and protein

* Corresponding author at: School of Medicine, Southern University of Science and Technology, Shenzhen, China.
** Corresponding author at: School of Basic and Forensic Medicine, Baotou Medical College, Baotou, China.
E-mail addresses: juhongge1088@163.com (H. Ju), wangyk@sustech.edu.cn (Y. Wang).
[1] These authors contributed equally to this work.

https://doi.org/10.1016/j.tranon.2024.101958
Received 6 December 2023; Received in revised form 22 March 2024; Accepted 8 April 2024

alterations known to be involved in the development, progression, and recurrence of bladder cancer with the purpose to diagnose and monitor bladder cancer [4,5]. Although progress has been achieved in treatments, the therapeutic effect is still not satisfactory, particularly for patients who have developed into advanced stages with distant metastasis, leading to poor clinical outcomes [6,7]. The progression of bladder cancer is a complicated process that is closely associated with abnormal genetic alterations [8]. Therefore, it is urgently necessary to identify novel biomarkers and find efficient therapeutic strategies for bladder cancer treatment.

Ubiquitination is a posttranslational modulation that exerts crucial roles in numerous cellular processes [9]. Protein ubiquitination can be reversed by a group of proteases known as deubiquitinating enzymes (DUBs). As reported, DUBs can remove the ubiquitin chains from ubiquitylated substrates to counteract the modification regulated by E3 ubiquitin ligases. The modification is essential for various biological events, including cell cycle and division, DNA transcription and repair, differentiation and development, immunoreaction, and cell apoptosis [10,11]. Ubiquitin-specific protease 21 (USP21) is a member of the USP family of DUBs and contains 56 members that are unified by a highly conserved USP domain [12,13]. USP21 is suggested to be highly expressed in a number of malignancies and is involved in varying malignant biological behaviors of tumors, thereby performing its oncogenic effects. For instance, high USP21 expression is associated with pancreatic ductal adenocarcinoma (PDAC) progression and enhances pancreatic cancer cell stemness through activating the Wnt signaling pathway [14]. USP21 is amplified in tumors from basal-like breast cancer (BLBC) patients, and its deficiency can sensitize breast cancer cell lines and mouse xenograft tumors to paclitaxel treatments via binding and deubiquitinating Forkhead Box M1 (FOXM1), herein improving chemosensitivity [15]. USP21 up-regulation could also enhance colorectal cancer metastasis through functioning as a Fra-1 deubiquitinase [16]. Recently, USP21 was reported to enhance the development of bladder carcinoma, initially providing evidence that USP21 could serve as a novel therapeutic target for bladder cancer treatment [17]. However, the underlying mechanisms require further exploration to find efficient therapeutic approaches.

Steroid hormones are (chole)sterol derivatives distributed in a mass of animals and plants, where they are involved in the modulation of various physiological processes [18]. 20-hydroxyecdysone (20-HE) is a type of polyhydroxylated steroid invertebrate hormone spread in insects and a few plants [19]. 20-HE has been increasingly focused on due to its beneficial pharmacologic properties for humans. Accordingly, 20-HE exerts hypolipidemic, anti-diabetic, antioxidant, anti-inflammatory, hepatoprotective, and anti-fibrotic effects [20–22]. For example, 20-HE could attenuate hepatic steatosis and decrease white adipose tissue mass in rodent animals receiving high fat and fructose [21]. Additionally, 20-HE mitigates collagen-induced arthritis by suppressing oxidative stress and inflammatory cytokines [22]. Additionally, 20-HE could significantly inhibit the proliferation of triple-negative breast cancer cells and induce pro-apoptotic activities [23]. More recently, 20-HE was shown to exert an anti-cancer role in human non-small cell lung cancer (NSCLC) cells via its antioxidant and antineoplastic properties [24]. These data revealed the anti-cancer potential of 20-HE; however, its regulatory functions during bladder cancer have not been explored and thus were investigated in our present work.

In the study, we reported that 20-HE markedly restrained the proliferation, EMT process, and lung metastasis in bladder cancer cells in vitro and in vivo. Intriguingly, we provided the first evidence that 20-HE could directly restrain the transcriptional expression levels of NF-κB/p65, and meanwhile function as an inhibitor of USP21, consequently resulting in proteasomal degradation of NF-κB/p65. These data establish a novel p65 gene suppression and protein degradation strategy regulated by 20-HE to develop efficient therapies for bladder cancer treatment.

Materials and methods

Antibodies and reagents

The primary antibodies used were shown as below: anti-Flag (#ab205606), anti-His (#ab18184), anti-Myc (#ab9106), anti-NF-κB/p65 (#ab16502), anti-phospho-NF-κB/p65 (#ab131100) anti-Caspase-3 (#ab13847), anti-GAPDH (#ab8245), anti-RRBP1 (#ab95983), CTNNB1 (#ab32572) and anti-Pan-cytokeratin (#ab7753) were obtained from Abcam (Cambridge, MA, USA); anti-HA (#3724), anti-N-cadherin (#13,116) and anti-KI-67 (#34,330) were purchased from Cell Signaling Technology (Beverly, MA, USA); anti-USP21 (#MA5–34,953; #PA5–116,440) was purchased from Thermo Fisher Scientific (Shanghai, China); anti-IKBKB (#AF7200) anti-PARP1 (#AG1047) were obtained from Beyotime Biotechnology (Shanghai, China); anti-Vimentin (#abs131996), anti-SRSF6 (#abs151893), anti-RAB21 (#ab101402), anti-FBXL14 (#abs153116), anti-RNF168 (#abs153663) were purchased from Absin Biotechnology (Shanghai, China). Secondary antibodies including Rabbit Anti-Mouse IgG H&L (HRP) (#ab6728) and Goat Anti-Rabbit IgG H&L (HRP) (#ab6721) were purchased from Abcam. Alexa Fluor 647-labeled Goat Anti-Mouse IgG($H+L$) (#A0473) and Alexa Fluor 488-labeled Goat Anti-Rabbit IgG($H+L$) (#A0423) were purchased from Beyotime Biotechnology. 20-hydroxyecdysone (also known as Crustecdysone; purity 99.63 %; #HY-N6979) and Chlorhexidine (CHX; #HY-B1248) were purchased from MedChemExpress (Shanghai, China). MG132 (#M7449) was obtained from Sigma Aldrich (St. Louis, MO, USA).

Cells and culture

The bladder cancer cell lines, including J82, 5637, T24, SW780, and UMUC3, and the normal human urothelial cell line, SV-HUC-1, were purchased from the American Type Culture Collection (ATCC; Manassas, VA, USA). The J82, UMUC3 and SW780 cell lines were cultured in Dulbecco's modified Eagle's medium (DMEM) (Gibco; Thermo Fisher Scientific). T24 and 5637 were fed in RPMI 1640 medium (Gibco), and SV-HUC-1 cell line was cultured in Ham's F-12 K medium (Gibco). All basic media were supplemented with 10 % fetal bovine serum (FBS; HyClone, USA) and 1 % penicillin/streptomycin (Gibco). All cells were maintained in an incubator at 37 °C with 5 % CO_2 and 95 % humidity. All cell lines have been authenticated by short tandem repeat (STR) profiling.

Cell proliferation analysis

Bladder cancer cells were seeded on a 96-well plate (2000 cells/well) for 24 h. Treated cells were then added 10 μl/well of CCK-8 reagent (#CA1210; Solarbio, Beijing, China) in a 37 °C incubator for 3 h. The OD value for the wavelength at 450 nm was read on a microplate reader (Thermo Multiskan GO, USA). For the EdU staining assay, the treated cancer cells were plated on 24-well plates with 8000 cells per well. Next, 10 μM EdU (#C0078L; Beyotime Biotechnology) was added to each well, and the plates were incubated for 2 h. Then, the cells were fixed with 4 % paraformaldehyde for 15 min and permeabilized using 0.3 % Triton X-100 (#T8200; Solarbio) for another 15 min. After incubation with click reaction buffer in the dark for 0.5 h, the cells were subjected to nuclei staining with 4′, 6-diamidino-2-phenylindole (DAPI, #C0065; Solarbio). Images were acquired using a fluorescence microscope (Nikon, Tokyo, Japan). As for the colony formation assay, 1000 cells per well were grown in 6-well plates with 2 mL of medium in each. After culture for 14 days at 37 °C in an incubator, 4 % polyoxymethylene was used for cell fixing. Then, the cells were stained with 0.1 % crystal violet, and images were finally captured under a light microscope (Nikon, Tokyo, Japan).

Wound healing assay

T24 and UMUC3 cells were seeded in 24-well plates. After incubation in FBS-free medium for 24 h, cancer cells were scraped using a pipette tip, and then added with full medium containing 10 % FBS with different concentrations of 20-HE. Photographs were taken by a micrograph at 0 and 24 h post wound-making under a microscope (Nikon). The percentage of wound closure areas was measured.

Plasmid construction and in vitro transfection

Bladder cancer cells were stably transfected with sh-USP21 or USP21 overexpression plasmids (Shanghai Bioscienceres. Co., Ltd., Shanghai, China). The negative shRNA (shCtrl) and empty vector were served as controls, respectively. Flag-tagged full-length USP21 (Flag-USP21) and Myc-tagged full-length p65 (Flag-p65) were generated from Obio Technology Co. (Shanghai, China) by standard PCR. The expression vectors of HA-Ubiquitin, HA-Ubiquitin K48-only, and HA-Ubiquitin K63-only were obtained from HedgehoBio Science and Technology (Shanghai, China). The pGLuc-Dura-SV40-C was obtained from Beyotime Biotechnology to obtain T24 cells stably expressing firefly luciferase. Transfection was performed using Lipofectamine 3000 transfection reagent (#L3000150; Invitrogen, Carlsbad, CA) following the manufacturer's instructions. Cells were infected with lentiviral and retroviral cDNA-expressing viruses, which were packaged in HEK293T cells, followed by puromycin (#HY-B1743A, MedChemExpress, Shanghai, China) treatment to screen stably infected cells. All constructed cell lines were cultured for no more than 6 months and tested for mycoplasma monthly.

Flow cytometry and Caspase-3 activity analysis

Apoptosis after 20-HE treatments was examined by Annexin V/propidium iodide (PI) staining using an Annexin V-FITC/PI apoptosis kit (#C1062L; Beyotime Biotechnology). Annexin V-FITC/PI staining was conducted according to the manufacturer's instructions, and the apoptosis rate was analyzed by flow cytometry (BD, Biosciences, USA).

Bladder cancer cells after treatments were collected and lysed to assess the Caspase-3 activity with a Caspase-3 Activity Assay Kit (#C1116; Beyotime Biotechnology). In brief, the lysates were harvested and measured for protease activity. After normalization, the cell lysates were added to each well of microplate with reaction buffer and substrate solution. Next, the microplate was incubated for 0.5 h at 37 °C and was read at OD405 nm on a microplate reader (Thermo Multiskan GO, USA).

RNA extraction and RT-qPCR analysis

Total RNA from cells was extracted using the TRIzol reagent (Invitrogen) following the manufacturer's protocols. RT-qPCR was conducted with a PrimeScript RT Reagent Kit (#RR036A, TaKaRa, Dalian, China) and a SYBR Premix Ex Taq (#RR620A, TaKaRa) according to the manufacturer's instructions on an ABI 7900 Real-time PCR system (Applied Biosystems, USA). PCR reaction for each was conducted in triplicate. Glyceraldehyde-3-phosphate dehydrogenase (GAPDH) was used as the loading control. Gene expression data were analyzed using the $2^{-\Delta\Delta Ct}$ method. The sequences for specific primers were listed in Table S1.

Western blot analysis

The extraction of total protein from tissues or treated cells was performed with radio-immunoprecipitation assay (RIPA) lysis buffer (#R0010; Solarbio). Then, the protein concentration was examined using a bichinconic acid (BCA) protein assay kit (#PC0020; Solarbio). An equivalent amount of protein was then loaded onto a 10 % sodium dodecyl sulphate-polyacrylamide gel (SDS-PAGE) before transferring the proteins onto 0.45 μm polyvinylidene fluoride (PVDF) membranes (#IPVH00010, Millipore). Next, 5 % non-fat milk in TBST was used for the membrane blocking for 1.5 h at room temperature, followed by incubation with primary antibodies at 4 °C overnight. After washing, corresponding secondary antibodies were subjected to the membranes for 1 h of incubation at room temperature. Signals were detected using enhanced chemiluminescence (ECL, #PE0010; Solarbio) as the manufacturer suggested. The protein expression levels were quantified using ImageJ software (NIH) and normalized to the relative internal standards.

Co-immunoprecipitation (IP) assay

Bladder cancer cells were harvested and lysed using NP-40 buffer (#N8032, Solarbio) containing a complete protease inhibitor cocktail (#P1006, Beyotime Biotechnology) on ice for 30 min. The obtained cell lysate was then centrifuged for 15 min at 12,000 rpm at 4 °C. The lysate supernatant was served as input, and the rest was cocultured overnight with Protein A/G Magnetic Beads (#P2179M, Beyotime Biotechnology) and the anti-USP21 or anti-p65 antibody on a shaking device at 4 °C. The corresponding IgG (Beyotime Biotechnology) was defined as the negative control. Subsequently, the magnetic beads were rinsed using cold NP-40 buffer and boiled for 10 min in loading buffer. After final centrifugation, the supernatant was harvested for western blot analysis with the primary antibodies as displayed.

Glutathione S-transferase (GST) pull-down assay

Human full-length USP21 cDNA was cloned into pGEX-5X-3vector, and the recombinant GST-USP21 protein was expressed in Rosetta (DE3) *Escherichia coli* cells (Yeasen, Shanghai, China) and purified using Glutathione Sepharose 4B beads (SEEBIO BIOTECH Co.,Ltd., Shanghai, China) for 1 h at 4 °C. Then, His-p65 (Proteintech Group, Inc., Wuhan, China) was incubated with either GST-USP21 or GST plus glutathione beads in the binding buffer at 4 °C overnight, followed by rinsing with the same buffer. Proteins were collected and boiled in SDS loading buffer for immunoblotting using anti-His-and anti-GST antibodies. Extracts from *E. coli* that only express the GST tag were used as the negative control.

Protein stability assay

Approximately 1×10^5 T24 and UMUC3 cells were seeded onto 12-well plates and transfected with Flag-USP21 or the vector. After 48 h, the cancer cells were treated with CHX (100 μg/ml) for the indicated times. Samples were then collected for western blot analysis to calculate p65 degradation condition.

In vivo ubiquitination assay

To examine the ubiquitination of p65, bladder cancer cells were co-transfected with Flag-USP21 (or vector), HA-Ub, HA-Ub-K48 or HA-Ub-K63 for 48 h. After exposure to the proteasome inhibitor MG132 (20 μM) for 8 h, the cell lysates were prepared using lysis buffer and immunoprecipitated with the shown antibody (anti-p65) on protein A/G beads (Beyotime Biotechnology) overnight. Subsequently, the beads were rinsed and boiled in SDS loading buffer. The supernatants were collected and immunoprecipitated with an anti-Myc antibody. Immunoblotting with an anti-HA antibody was conducted to detect p65 polyubiquitination.

Immunofluorescence (IF)

For the IF staining assay, cells were fixed with 4 % paraformaldehyde at room temperature for 15 min and then permeated with 1 % Triton X-100 (#T8200; Solarbio) for 15 min and washed with PBS. Next, the cells

were blocked using 3 % bovine serum albumin (BSA, #A8010; Solarbio) for 1 h at 37 °C. After washing, the cells were incubated with primary antibodies against anti-USP21, anti-p-NF-κB/p65, or anti-NF-κB/p65 overnight at 4 °C, followed by incubation with an Alexa Fluor®488-conjugated secondary antibody for 45 min at 37 °C. The nuclei were counterstained using DAPI (#C0065; Solarbio) for 5 min at room temperature. Finally, images were obtained under a confocal microscope (Olympus, Japan).

Animal studies

Animal studies were performed with the approval of the Institutional Animal Care and Use Committee at the Southern University of Science and Technology (Shenzhen, China) and in line with the National Guidelines for the Experimentation of Animals. The 4-week-old male Balb/c nude mice (weighing 18–20 g; Guangdong Medical Laboratory Animal Center, Guangdong, China) were housed in laminar flow cabinets under specific pathogen-free (SPF) conditions with a 12-h light/12-h dark cycle and given food and water ad libitum. All mice were randomly divided into 4 groups, including the control group, mice receiving the 20-HE low dosage group ($L = 2.5$ mg/kg), mice receiving the 20-HE medium dosage group ($M = 5$ mg/kg), and mice receiving the 20-HE high dosage group ($H = 10$ mg/kg). A total of 1×10^7 T24 cells were subcutaneously injected into the left or right flank of the axilla of each animal. When the tumors reached 100 mm^3 in volume, 20-HE (2.5, 5, or 10 mg/kg) dissolved in vehicle (olive oil plus DMSO that was not exceeding 10 % of volume injected) was subjected to mice by gavage daily. The control group of mice only received the vehicle. A vernier caliper was used to examine the length and width of the tumors weekly, and tumor volume was assessed with the formula $(L \times W^2)/2$. After 5 weeks, the body weights of mice were recorded. Then, these mice were sacrificed, and blood was collected for toxicity analysis. Then, all subcutaneous tumors were dissected and weighed. Major organs, including livers, hearts, kidneys, lungs, and spleens from all groups of mice were excised and fixed in 4 % paraformaldehyde for hematoxylin and eosin (H&E) staining to examine tumor morphology and immunohistochemical calculation.

For the lung metastasis assay, T24 cells (1×10^7) were injected into the tail vein of the male Balb/c nude mice ($n = 4$ for each group). Different dosages of 20-HE (2.5, 5, or 10 mg/kg) were administered to mice daily by gavage, as described in the above xenograft mouse models. The vehicle was given to the control group of mice orally. After treatment for 6 weeks, mice were sacrificed, and the number of metastatic nodules on the excised lung was counted. Then, the lung tissues were fixed in 4 % paraformaldehyde for H&E staining. Additionally, to confirm the potential of 20-HE on lung metastasis, in vivo imaging system (IVIS) was further used. In brief, T24 cells (1×10^7) stably expressing firefly luciferase mice were subjected to the male Balb/c nude mice ($n = 4$ in each) via the tail vein. Six weeks later, all mice were injected with 15 mg/ml D-luciferin (Beyotime Biotechnology), and metastatic progression was monitored and quantified using the in vivo imaging system Spectrum (Xenogen Corp./Caliper life Science, Alameda, CA, USA). The quantification of tumors in each image is relative to the total tissue area and is presented as a percentage, that is, tumor-to-lung ratio = [tumor area/tumor + healthy surrounding tissue area] × 100.

We further established an inguinal lymph node metastasis model to investigate the potential of 20-HE on bladder cancer progression. Briefly, T24 cells (2×10^6/50 μl PBS/mouse, $n = 4$ in each group) stably expressing firefly luciferase were injected into the foot pads. Then, tumor-bearing mice were randomly divided into three groups treated with 20-HE (5 or 10 mg/kg) daily by gavage. These mice receiving saline were defined as the control group. Lymph node volume was measured weekly and evaluated by the formula: length × $width^2$ × 0.5. After 28 days, 15 mg/ml D-luciferin (Beyotime Biotechnology) diluted in PBS was then intraperitoneally injected at a dose of 10 ul/g. Fluorescence imaging of nude mice was then performed. Next day, mice were sacrificed after injection of pentobarbital sodium. Primary tumor in foot pad and inguinal lymph nodes were removed for further analysis.

Biochemical parameters assay

The contents of serum alanine aminotransferase (ALT; #C009–2–1), aspartate aminotransferase (AST; #C010–2–1), urea nitrogen (BUN; #C013–2–1) and creatine kinase (CK; #A032–1–1) in each group of mice were measured by the use of commercially available kits following the instructions provided by the supplier (Nanjing Jiancheng Bioengineering Institute, Nanjing, China).

Immunohistochemistry staining (IHC)

Tumor tissues were fixed in 4 % paraformaldehyde for at least 2 days at room temperature. Then, the samples were paraffin embedded and sectioned at 5 μm-thick. Sections for IHC staining were heated at 65 °C for 2 h, deparaffinized in xylene and hydrated in graded alcohol. Endogenous peroxidase activity was then eliminated by 3 % hydrogen peroxide. After antigen retrieval, the sections were blocked in BSA solution (Solarbio) for 20 min. Subsequently, the slides were incubated with primary antibodies at 4 °C overnight, including anti-KI-67, anti-N-cadherin, anti-USP21, anti-p-NF-κB/p65 and anti-NF-κB/p65. After washing with PBS, the sections were incubated with corresponding secondary antibodies for 45 min at room temperature. Finally, the tumor sections were stained with diaminobenzidine (DAB) for 5 min and mounted with hematoxylin. The images were photographed under a microscope (Nikon, Japan).

TUNEL staining

In order to detect tumor apoptosis, TUNEL staining was performed. The fixed tumor tissues were embedded in paraffin and 5-μm-thick sections were deparaffinized by washing in xylene and a descending ethanol series. The sections were subsequently incubated with 20 μg/mL proteinase K for 30 min at 37 °C, and endogenous peroxidase was inactivated by 3 % H_2O_2 in methanol for 10 min. They were incubated with 50 μL of a TUNEL reaction mixture (Beyotime Biotechnology) on the section for 60 min at 37 °C, and then 50 μL converter-POD was added to the sample for 30 min at 37 °C. For color development, sections were supplement-ed with 50 μL DAB substrate for 10 min at room temperature to detect labeled nuclei, and then counterstained by hematoxylin. For each slide, 5∼10 separate fields were examined randomly and digitized by microscopy. The apoptotic index was calculated as the ratio of TUNEL-positive cells to the total number of cells.

Bioinformatic analysis

The expression levels of USP21 in bladder cancer tumors and normal tissues, and its expression profiles in the clinical stages of patients with bladder cancer were analyzed based on the TCGA database. Spearman correlation among USP21, RELA and NFKBIB in patients with bladder cancer was also explored by the use of TCGA database. RNA sequencing was performed by Novogene Technology (Beijing, China) for high-throughput sequencing. Total RNA was extracted from T24 cells treated with or without 20-HE (10 μM) using Trizol (TaKaRa). Differential gene expression was identified by raw read counts via DESeq2 [25]. Differentially expressed genes (DEGs) were screened following the criteria that $|\log2(\text{FoldChange})| > 1$ and adjusted $p < 0.05$. Gene Ontology (GO) biological process gene sets and the Kyoto Encyclopedia of Genes and Genomes (KEGG) database were used to calculate the protein family and signaling pathway. Summary of protein-protein interaction network and MCODE components identified in the DEGs was performed by metascape (https://metascape.org). The volcano plot and heat-map diagram were drawn using R software.

Liquid chromatography tandem mass spectrometry (LC-MS/MS)

The Flag-USP21 were transfected into T24 cells. Anti-Flag affinity magnetic beads were used for immunoprecipitation. The proteins were then identified and subjected to mass spectrometry as previously described [26,27]. Briefly, protein extracted from H1299 cells was used as input control and for immunoprecipitation. Sample was incubated with anti-Flag antibody and 50 μl agarose A protein overnight at 4 °C.

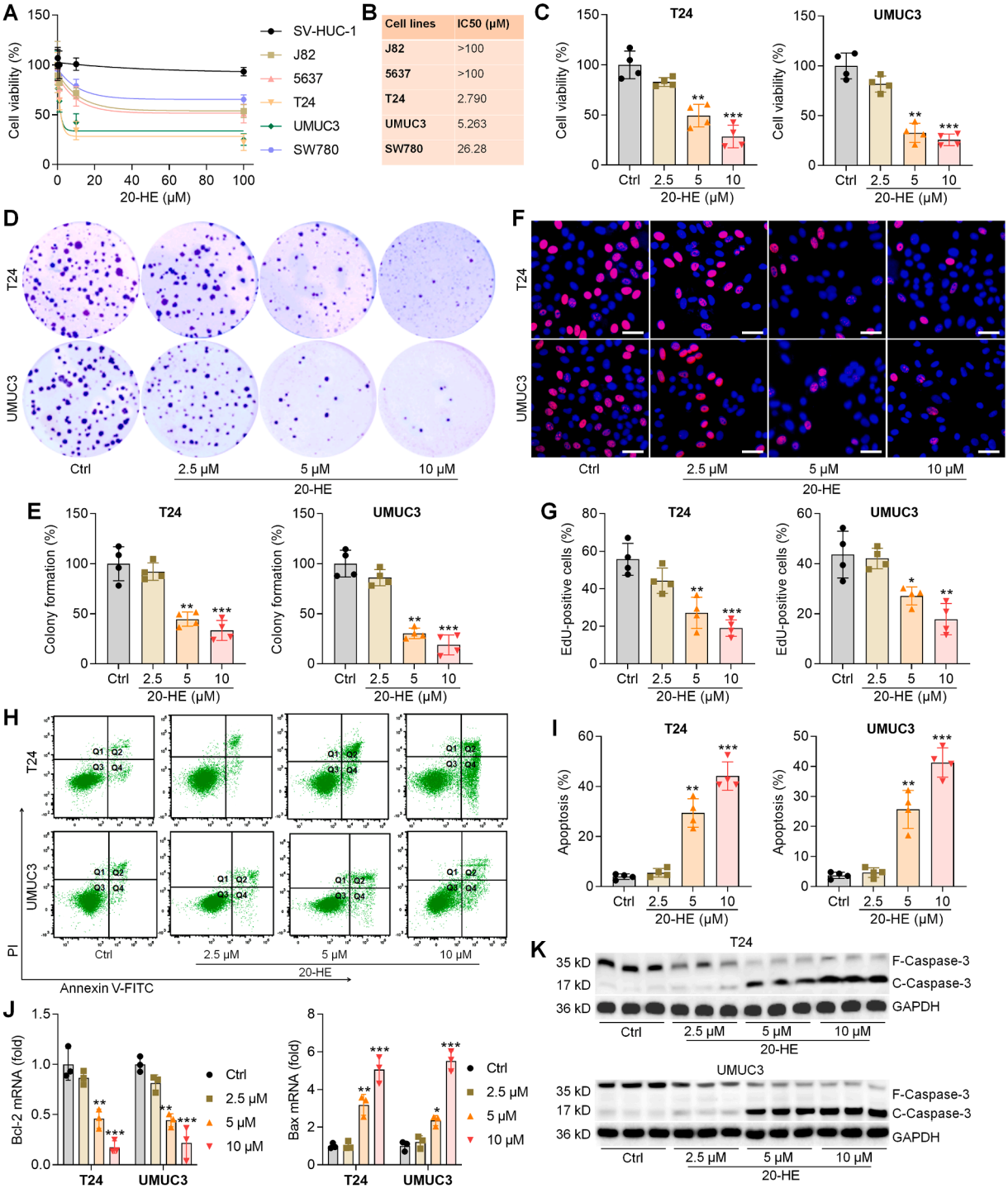

Fig. 1. 20-hydroxyecdysone inhibits the proliferation and induces apoptosis in bladder cancer cells. (A) Several bladder cancer cell lines (J82, 5637, T24, UMUC3 and SW780) and normal human urothelial cell line (SV-HUC-1) were incubated with different concentrations (from 0 to 100 μM) of 20-HE for 24 h. Then, all cells were collected for cell viability calculation using CCK-8 analysis. (B) IC_{50} for each cell line was quantified and shown. (C-K) Bladder cancer cell lines T24 and UMUC3 were incubated with 20-HE (2.5, 5 or 10 μM). After treatment for 24 h, T24 and UMUC3 cells were harvested for studies as below. (C) Cell viability quantification by CCK-8 assay. (D&E) Colony formation and (F&G) EdU staining analysis were performed to examine the proliferation of bladder cancer cells (Scale bar = 50 μm). Quantification for each was displayed. (H&I) Apoptosis of bladder cancer cells was measured using flow cytometry analysis. (J) RT-qPCR analysis for Bcl-2 mRNA expression levels. (K) Western blot results for cleaved Caspase-3 protein expression levels. Data are displayed as mean ± SD ($n = 3$ or 4 in each group). $^{*}p < 0.05$, $^{**}p < 0.01$ $^{***}p < 0.001$ *vs* the Ctrl group.

The Flag-beads (Thermo Fisher Scientific) were washed with lysis buffer and boiled in SDS sample buffer, and the pulled-down protein was separated on SDS-PAGE gels. Then, the gels were stained with Coomassie Blue, and differentially abundant bands were cut out for mass spectrometry using LTQ Orbitrap Elite (Thermo Fisher) and a Waters NanoAcquity HPLC pump (Milford, MA, USA).

Statistical analysis

All data are expressed as the mean ± standard deviation (SD) with at least three biological replicates. Statistical data analysis was performed with GraphPad Prism (version 9.2.0, GraphPad Software, San Diego, CA, USA). Differences between groups were examined using the two-tailed Student's *t*-test or one-way analysis of variance. The correlation between two variables was evaluated by Pearson's correlation analysis. A $p < 0.05$ was considered statistically significant.

Results

20-hydroxyecdysone inhibits the proliferation and induces apoptosis in bladder cancer cells

We first conducted a proliferation analysis to evaluate the sensitivity of bladder cancer cells to 20-HE. The results showed that the suppressive effects of 20-HE on bladder cancer cells were dose-dependent, particularly in the T24 and UMUC3 cell lines, with IC50s of 2.790 and 5.263 μM, respectively (Fig. 1A and B). Given that T24 and UMUC3 cell lines were the more sensitive to 20-HE treatments than that of other three

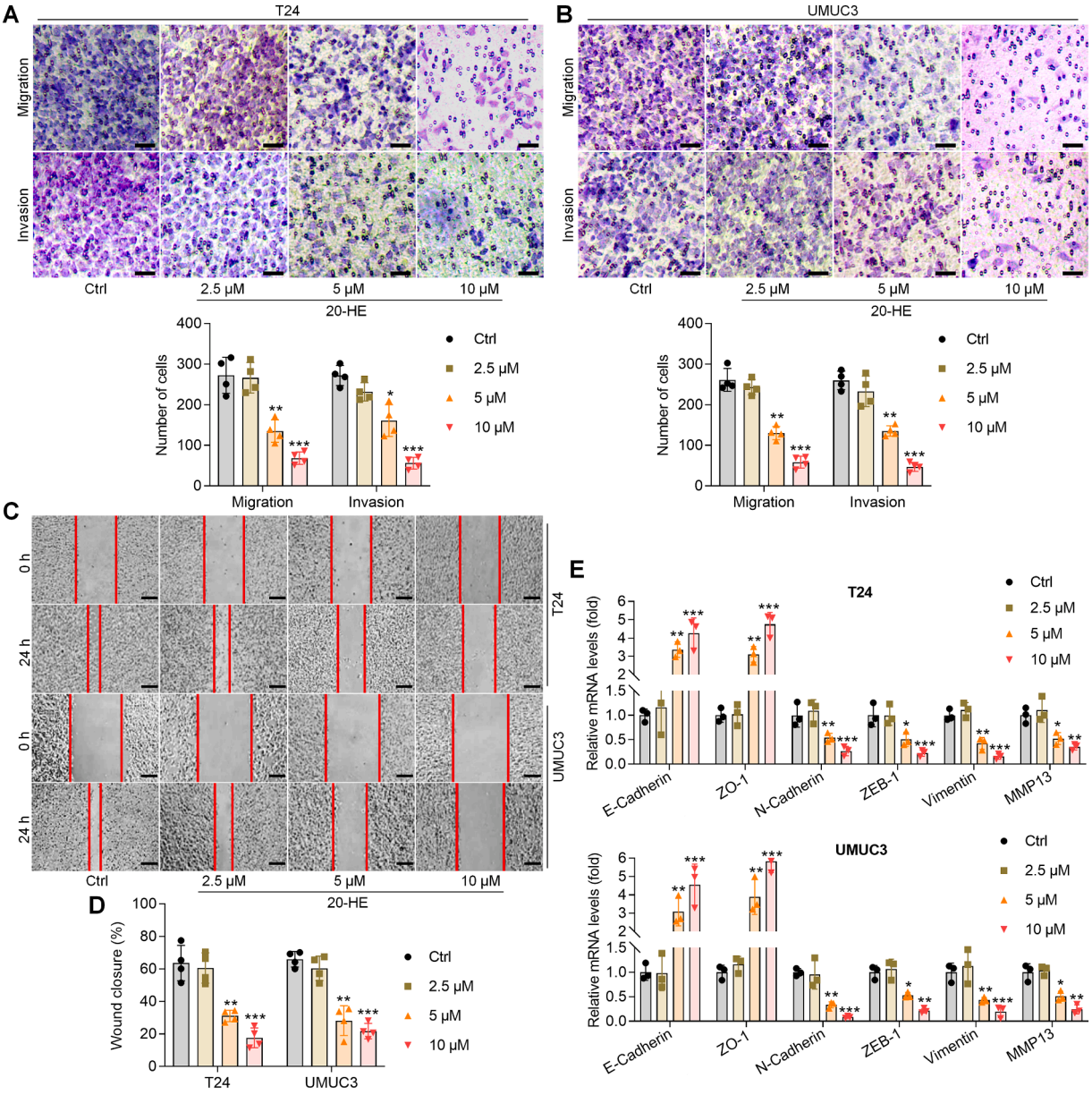

Fig. 2. 20-hydroxyecdysone suppresses the migration and invasion in bladder cancer cells. (A-E) T24 and UMUC3 cells were exposed to 24 h of 20-HE (2.5, 5 or 10 μM), and were then harvested for studies as follows. (A&B) Transwell assay was conducted to examine the migratory and invasive properties of bladder cancer cells (Scale bar = 50 μm). The number of cells in migration and invasion was quantified and listed. (C) Wound closure healing analysis was used to examine the migration of bladder cancer cells (Scale bar = 100 μm). (D) The percentage of wound closure for each condition was quantified. (E) RT-qPCR analysis was conducted to examine the mRNA expression changes of EMT markers, including E-Cadherin, ZO-1, N—Cadherin, ZEB-1, Vimentin and MMP13. Data are displayed as mean ± SD ($n = 3$ or 4 in each group). $^{*}p < 0.05$, $^{**}p < 0.01$ $^{***}p < 0.001$ *vs* the Ctrl group.

ones with much lower IC50 values, they were selected for subsequent studies. The CCK-8 analysis further identified that cell viability was markedly decreased with an increase in 20-HE concentration (Fig. 1C). Colony formation and EdU staining assays demonstrated that the clone numbers (Fig. 1D and E) and EdU-positive cells (Fig. 1F and G) were significantly down-regulated in bladder cancer cells with 20-HE exposure in a dose-dependent manner. Flow cytometry analysis in Fig. 1H and I indicated that 20-HE strongly induced apoptosis in T24 and UMUC3 cells. RT-qPCR results showed that anti-apoptotic marker Bcl-2 expression levels were highly down-regulated in T24 and UMUC3 cells with 20-HE incubation (Fig. 1J). As expected, 20-HE treatment markedly increased cleaved Caspase-3 expression levels and its activation in

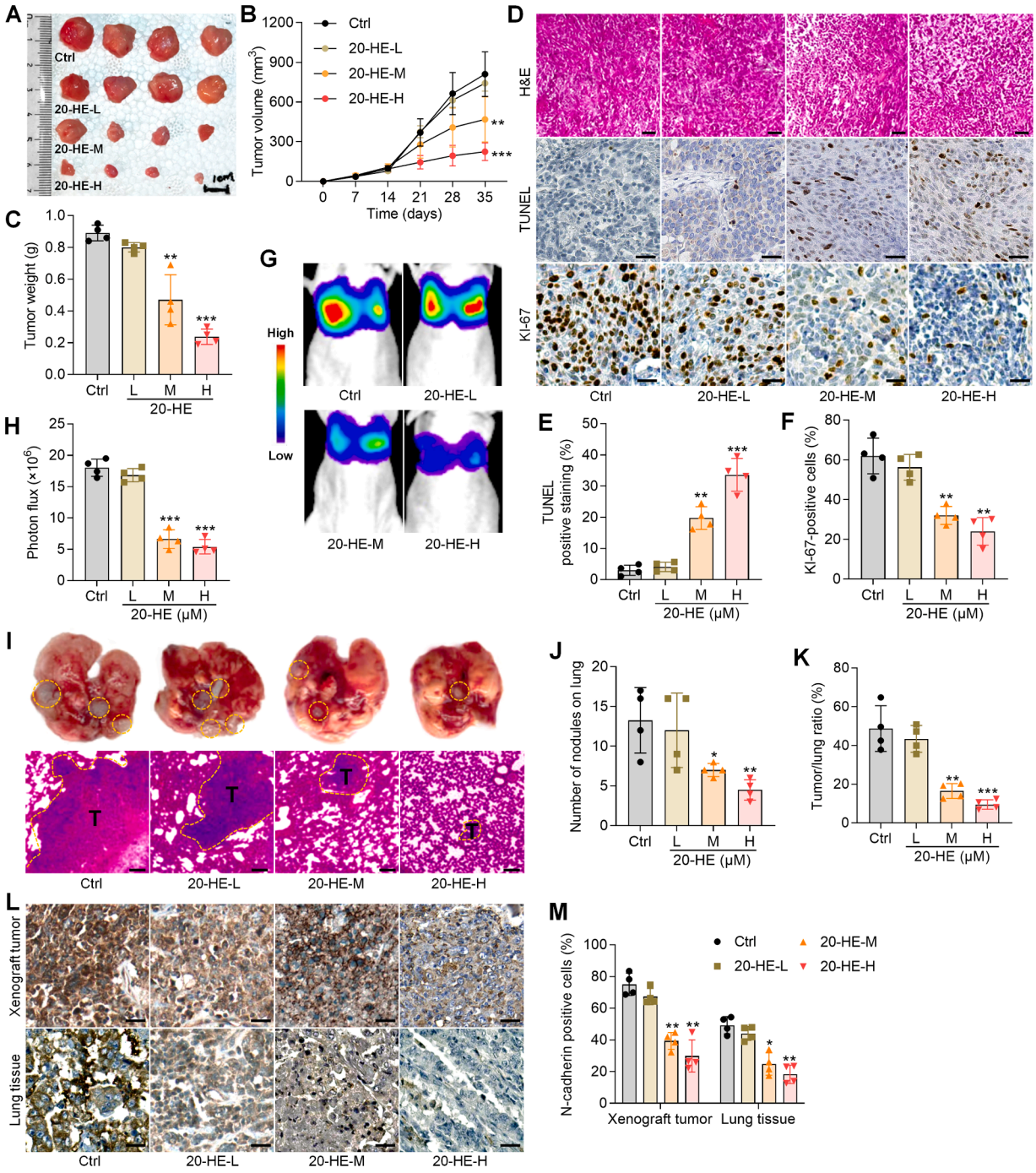

Fig. 3. 20-hydroxyecdysone reduces tumor growth and metastasis in the xenograft mouse model of bladder cancer. (A) Tumor samples from each group were shown. (B) Tumor volume was measured. (C) Tumor weights were recorded. (D) H&E staining (Scale bar = 100 μm), TUNEL staining (Scale bar = 50 μm) and IHC staining for KI-67 (Scale bar = 50 μm) expression calculation in tumor sections. Quantification for (E) TUNEL and (F) KI-67 positive cells was displayed. (G) Lung metastases that developed in the T24 cell lines using an IVIS imaging system. (H) Representative luciferase signals were captured and analyzed. (I) Lung tissues (up) and H&E staining of pulmonary tissues (down; Scale bar = 200 μm) were displayed. Tumor area was marked by the yellow dotted line. (J) The number of nodules on lung tissues was examined. (K) Tumor-to-lung ratios were examined. (L) IHC staining for N-cadherin in the tumor tissues from xenograft mouse model and lung metastasis model was conducted (Scale bar = 50 μm). N-cadherin positive expression levels were quantified. Data are displayed as mean ± SD ($n = 4$ in each group). $^{*}p < 0.05$, $^{**}p < 0.01$ $^{***}p < 0.001$ *vs* the Ctrl group (For interpretation of the references to color in this figure legend, the reader is referred to the web version of this article).

bladder cancer cells in a concentration-dependent fashion (Fig. 1K and Fig. S1A and B), supporting the inhibitory effects of 20-HE on bladder cancer progression by triggering apoptosis.

20-hydroxyecdysone suppresses the migration and invasion in bladder cancer cells

Subsequently, we examined whether 20-HE could restrain the metastatic ability of bladder cancer cells. After 20-HE coculture, the transwell analysis showed that the number of bladder cancer cells that were migrating and invading was clearly lower (Fig. 2A and B). A wound healing assay confirmed the function of 20-HE to limit the migratory ability of bladder cancer cells in a dose-dependent manner (Fig. 2C and D). The expression levels of EMT-associated hallmarks, including N—Cadherin, ZEB-1, Vimentin, and matrix metalloproteinase-13 (MMP13), were greatly reduced by 20-HE, while E-cadherin and ZO-1 expression levels were improved in a dose-dependent manner (Fig. 2E). Together, these data initially suggested that 20-HE treatment exerted a dose-dependent suppressive effect on the proliferation and metastasis ability of bladder cancer cells in vitro.

20-hydroxyecdysone reduces tumor growth in the xenograft mouse model of bladder cancer

We then constructed an animal model to further examine the effect of 20-HE on the tumorigenesis of bladder cancer in vivo. The results showed that 20-HE treatments significantly suppressed tumor growth compared with the control group, as indicated by the reduced tumor growth rates, size, and weights in a dose-dependent manner (Fig. 3A-C). Subsequently, H&E staining showed that majority of cancer cells were damaged in the groups of mice receiving mild moderate dose and high dose of 20-HE treatments, such as nucleus or cell membrane damage, accompanied by decreased tumor cell density. In addition, results by TUNEL staining indicated that 20-HE at higher dosages markedly induced cell death in tumor sections compared with the Ctrl group (Fig. 3D and E). IHC staining indicated that 20-HE administration markedly reduced the positive expression of KI-67 in tumor tissues compared to the control mice, confirming the inhibitory effect of 20-HE on the proliferation of bladder cancer cells (Fig. 3D and F). We then performed IVIS and the bioluminescent imaging for metastasis extension showed that signal indicative of metastatic growth in the pulmonary regions of all groups; however, mice with mild moderate dose and high dose of 20-HE administration exhibited a tendency for decreased metastatic expansion signals (Fig. 3G and H). Consistently, the anatomy and H&E staining confirmed that 20-HE administration markedly restrained the bladder cancer cell lung metastasis via a concentration-dependent fashion, as evidenced by the reduced number of nodules on lung tissues and decreased tumor/lung ratios (Fig. 3I-K). Additionally, N-cadherin positive expression levels were consistently found to be down-regulated by 20-HE treatments in xenograft mouse models and lung metastasis tumor tissues (Fig. 3G). To further explore the effect of 20-HE on distant organ metastasis, we established a mouse model with lymphatic metastasis in bladder cancer by injecting T24 cells into the foot pad of mice (Fig. S2A). We found that mice with 20-HE treatment exerted smaller foot pad tumor and metastatic tumor compared with the control group (Fig. S2B and S2C). Fluorescence imaging was performed after 28 days of feeding, and results analysis showed that luminescence area was strongly reduced in mice treated with 20-HE (Fig. S2D and S2E). Then, metastatic cells were evaluated in the lymph nodes by H&E and IHC staining, and results showed fewer lymph node metastases in 20-HE treated groups, along with lower Pan-cytokeratin positive cells and reduced lymph node metastasis rates (Fig. S2F and S2G). Moreover, significantly reduced expression levels of N-cadherin were detected in the foot pad tumor sections (Fig. S2H). These results above elucidated that 20-HE could inhibit tumor growth and restrain lung metastasis and lymph metastasis in vivo, contributing to the suppression of bladder cancer progression.

Given the anti-tumor potential of 20-HE in bladder cancer, we subsequently attempted to explore whether 20-HE exerted toxicity in mice. As shown in Fig. S3A, different concentrations of 20-HE had no significant influence on the body weight changes among all groups of mice. In addition, compared to the Ctrl group of mice, there were no obvious histological changes observed in the major organs of mice receiving 20-HE treatments by H&E staining (Fig. S3B). Similar contents of serum ALT, AST, BUN, and CK were detected in all groups of mice (Fig. S3C), further revealing that 20-HE had no hepatic, renal, or cardiac toxicities in mice. Taken together, these findings illustrated that 20-HE exerted repressive influences on proliferation and metastasis to restrain bladder cancer pathogenesis.

The enrichment analysis of DEGs mediated by 20-hydroxyecdysone in bladder cancer cells, and USP21 expression changes in bladder cancer patients

Through the RNA-seq analysis, we found that 100 mRNAs were differentially expressed after 20-HE treatment ($\log2FC > 1$, $p < 0.05$). Volcano plot and heat-map results indicated that most of these genes were decreased, including Collagen 1A1 (COL1A1), transforming growth factor-β1 (TGFB1), MMP13, SMAD7, RELA (NF-κB/p65), NFKB inhibitor beta (NFKBIB), and USP21, while these genes, including CASP3, CDH1 (E-cadherin), and BAX, were increased (Fig. 4A and B). Bioinformatic analysis was conducted to explore the functions of the genes associated with 20-HE-restrained bladder cancer. GO analysis indicated that the genes associated with the suppressive role of 20-HE in bladder cancer were enriched in the collagen-containing extracellular matrix and fibronectin binding. KEGG pathway analysis showed that the genes were mainly involved in bladder cancer-associated signaling pathways (Fig. 4C and Table S2). The chord dendrogram and bubble diagram listed the enriched GO terms and KEGG pathways, such as RELA, BAX, BCL2, MMP2, CDH2 (N—Cadherin), TP53, epidermal growth factor receptor (EGFR), and vascular endothelial growth factor A (VEGFA) (Fig. 4D and E), which were closely associated with the progression of cancer cell proliferation and EMT [28,29]. Metascape analysis (https://metascape.org/gp/index.html) confirmed these above protein-protein interaction networks and MCODE components for the enriched terms of DEGs (Fig. 4F and G). Ubiquitination is a post-translational regulation that plays essential roles in various cellular processes, including tumor growth [9]. Aberrant expression of USP family members is closely associated with cancer cell proliferation and a series of malignant biological behaviors of cancers [10,11]. Results from the volcano plot and heat map showed a significant decrease in USP21 in bladder cancer cells after 20-HE treatment, disclosing its potential for 20-HE-suppressed tumor growth. Analysis of the TCGA public dataset suggested that USP21 was markedly upregulated in patients with bladder cancer compared with the normal group (Fig. 4H), regardless of tumor stages (Fig. 4I) and histological types (Fig. 4J). Additionally, positive correlations among USP21, RELA, and NFKBIB were observed in patients with bladder cancer (Fig. 4K and L). Together, these bioinformatic analysis results suggested that USP21 up-regulation participated in bladder cancer progression, and its expression suppression might be associated with bladder cancer inhibition mediated by 20-HE.

20-hydroxyecdysone down-regulates USP21 expression levels in bladder cancer

In this section, we consistently found that 20-HE treatments dose-dependently reduced USP21 gene and protein expression levels in T24 and UMUC3 cells (Fig. 5A and B). IF staining confirmed the results that 20-HE could obviously down-regulate USP21 expression levels in bladder cancer cells (Fig. 5C and D). As expected, tumors from the xenograft mouse model exerted markedly decreased expression of USP21 by RT-qPCR, western blot, and IHC staining assays (Fig. 5F-G).

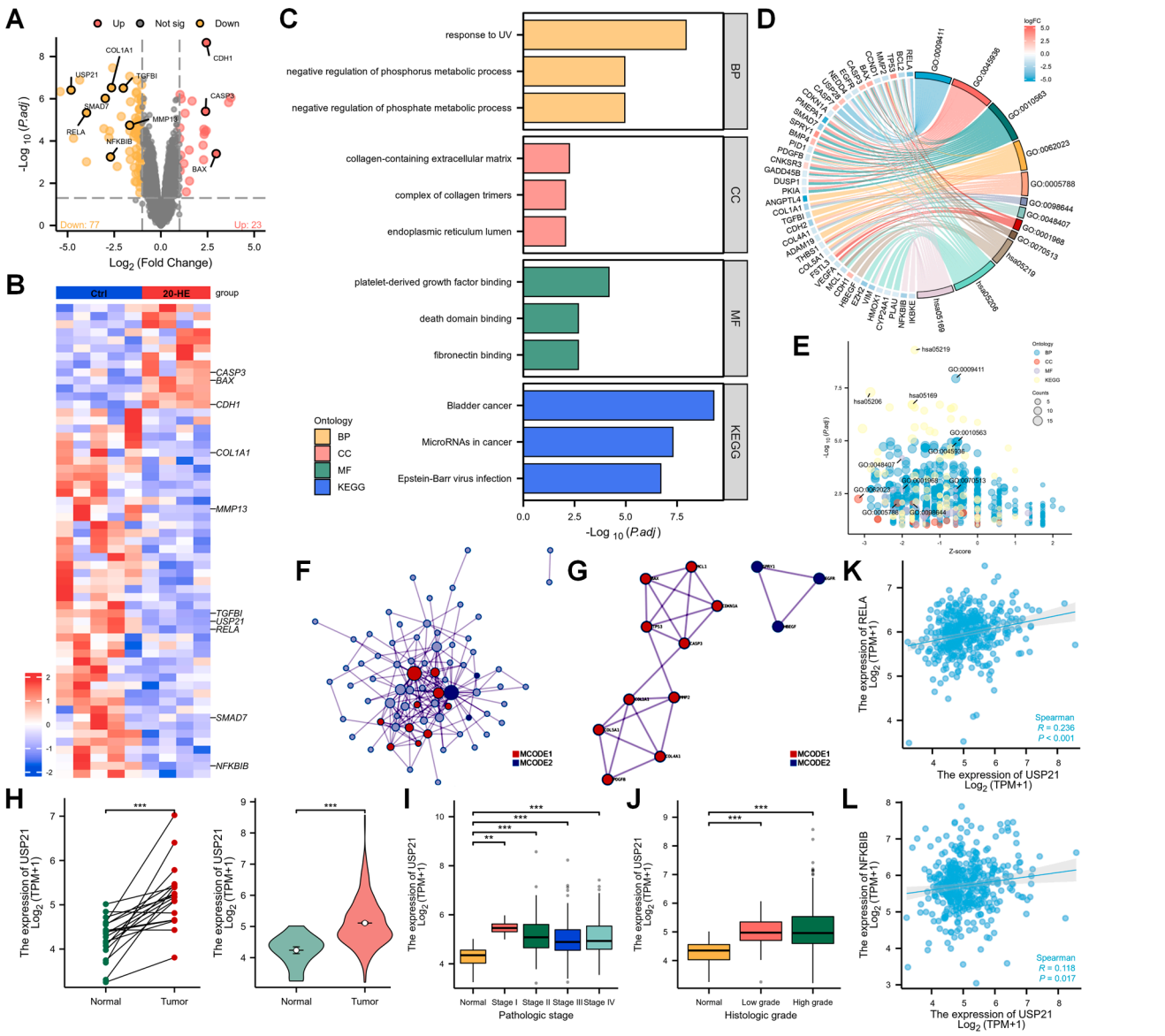

Fig. 4. The enrichment analysis of DEGs mediated by 20-hydroxyecdysone in bladder cancer cells, and USP21 expression changes in bladder cancer patients. (A) Volcano plots for DEGs of 20-HE-treated (10 μM) vs Ctrl group in T24 cells. (B) Heat map showing the expression of DEGs in the 20-HE and Ctrl group in T24 cells. (C) Biological Process (BP) terms, Cellular Component (CC) terms, Molecular Function (MF) terms and KEGG analysis of RNA sequencing data for the bladder cancer cell line T24 (20-HE vs Ctrl). (D) Chord dendrogram and (E) bubble diagram indicating a top GO cluster plot of the expression spectrum of significantly expressed genes. (F&G) Protein-protein interaction network and MCODE components for enriched terms of DEGs in T24 cells (20-HE vs Ctrl) using Metascape online assay system. (H) USP21 expression levels in tumor samples and normal tissues from patients with bladder cancer by the use of TCGA database. (I&J) USP21 expression levels in bladder cancer patients at different pathologic stages or histologic grades based on TCGA dataset. (K&L) Correlation between the gene expression of USP21 and RELA (p65) and NFKBIB in bladder cancer patients by the TCGA database. Data are displayed as mean ± SD (n = 4 or 5 in each group).

These in vitro and in vivo findings demonstrated that 20-HE could restrain USP21 expression in bladder cancer.

20-hydroxyecdysone reduces NF-κB/p65 stability in bladder cancer

Bioinformatic results above showed that NF-κB/p65 (RELA) had a positive correlation with USP21 in patients with bladder cancer, and its reduction was observed in 20-HE-incubated bladder cancer cells. To confirm our findings, western blot and IF staining assays were further performed. As shown in Fig. 6A and B, the transcriptional levels and protein expression levels of NF-κB/p65 and its phosphorylation were markedly down-regulated by 20-HE in T24 and UMUC3 cells in a dose-dependent fashion. Clearly mitigated expression levels of p-NF-κB/p65 and NF-κB/p65 were identified in bladder cancer cells after 20-HE exposure by IF staining (Fig. 6C and D). We also detected markedly decreased expression of p-NF-κB/p65 and NF-κB/p65 in the dissected xenograft tumor tissues from mice with 20-HE administration (Fig. 6E). Together, these data revealed that 20-HE exhibited suppressive effects on NF-κB/p65 expression and its phosphorylation in bladder cancer.

USP21 directly interacts with p65 and maintains its stability in bladder cancer cells, which can be abrogated by 20-hydroxyecdysone

The p65 is closely linked to cell survival, invasion, metastasis, and angiogenesis [30]. Ubiquitination of p65 has a key role in modulating its function [31]. USP21 has oncogenic functions in various types of human cancers by regulating the stability and degradation of its multiple substrate proteins [12]. Herein, whether USP21 could control p65

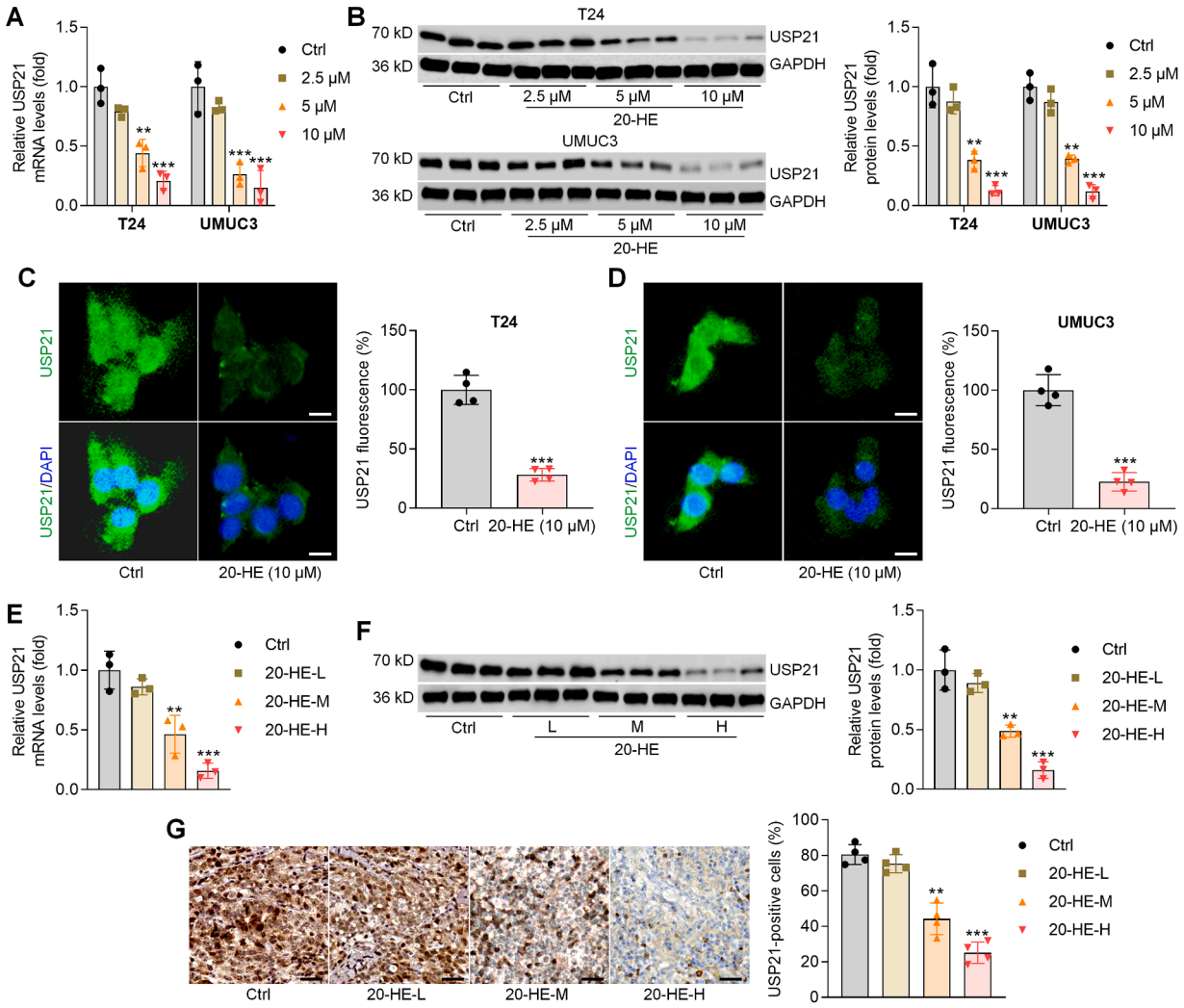

Fig. 5. 20-hydroxyecdysone down-regulates USP21 expression levels in bladder cancer. (A-D) T24 and UMUC3 cells were incubated with 20-HE (2.5, 5 or 10 μM) for 24 h, and were then harvested for following experiments. (A) RT-qPCR and (B) western blot assays were used to examine USP21 gene and protein expression levels. (C&D) IF staining was conducted to assess USP21 expression in T24 and UMUC3 cells (Scale bar = 15 μm). (E) USP21 mRNA and (F) protein expression levels in xenograft tumor samples were measured by RT-qPCR and western blot analysis, respectively. (G) IHC staining was included to examine USP21 positive expression levels in tumor tissues (Scale bar = 50 μm). Data are displayed as mean ± SD ($n = 3$ or 4 in each group). $^{**}p < 0.01$ $^{***}p < 0.001$ *vs* the Ctrl group.

stabilization in bladder cancer was investigated to further uncover the underlying mechanism of 20-HE in the treatment of bladder cancer. First, USP21 expression was knocked down in T24 and UMUC3 cells by transfecting with shUSP21, and we examined the efficiency of shUSP21 by RT-qPCR and western blot assays (Fig. 7A and B). Notably, p65 protein expression levels were also ameliorated by shUSP21 in bladder cancer cells. However, USP21 knockdown showed no significant influence on the changes in p65 mRNA expression levels (Fig. 7C), indicating that USP21 could regulate p65 stability at the post-transcriptional level rather than the transcriptional level. We then used Co-IP with antibody against USP21 and affinity enrichment followed by high-resolution LC-MS/MS analysis to determine how USP21 influences biological functions in bladder cancer cells. The T24 cell line was used, and the cells were divided into two groups, T24-USP21 and T24-Vector to identify USP21-binding proteins (Fig. 7D). In total, 235 and 309 proteins were identified as the USP21 interactome in T24-vector and T24-USP21 cells, respectively. Among them, 73 proteins in the two cell lines examined were found to overlap. When the quantification ratio of >2 was set as the interactive protein threshold, top ten proteins were identified as possibly showing enhanced interaction with USP21 when USP21 was overexpressed in T24 cells (Fig. 7E). Combine with the results of mass spectrum, the top 10 candidates were included and tested individually by the IP assay. Of these, only RELA validated as interacting with USP21 (Fig. 7F). We then confirmed the interactions between USP21 and p65 by co-IP in T24 and UMUC3 cells (Fig. 7G). GST pull-down analysis further showed that USP21 directly interacted with p65 in T24 and UMUC3 cells (Fig. 7H). Moreover, IF staining assays revealed that USP21 and p65 were highly colocalized in the nucleus and cytoplasm of bladder cancer cells (Fig. 7I). Additionally, p65 protein expression levels were increased in bladder cancer cells by USP21 in a dose-dependent manner (Fig. 7J). To further examine the effects of USP21 on p65 stability, bladder cancer cells were treated with the protein synthesis inhibitor CHX. Promoting USP21 expression markedly weakened the degradation of p65 protein in T24 and UMUC3 cells (Fig. 7K). Taken together, USP21 directly interacted with p65 and maintained its stability in bladder cancer cells.

The deubiquitination influence of USP21 on p65 was then calculated in bladder cancer cells. Ubiquitin-overexpressed plasmids were transfected into the T24 and UMUC3 cells, and the p65 ubiquitination status was measured. Western blot results in Fig. 7L indicated that the ubiquitination of p65 was evidently suppressed when USP21 was overexpressed. Additionally, similar results were detected in the presence or absence of the proteasome inhibitor MG132. Subsequently, we examined which type of ubiquitination modification of p65 was removed by

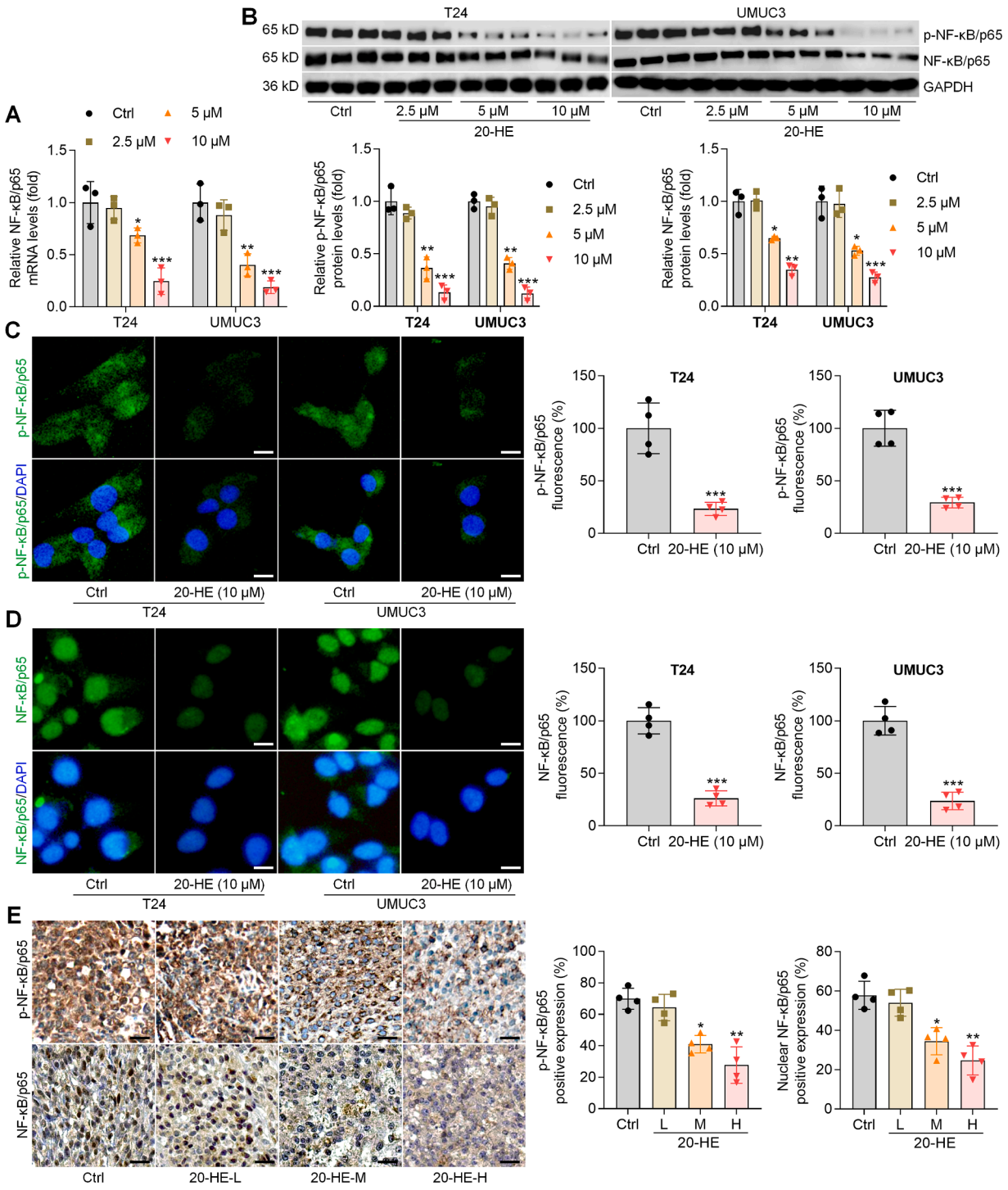

Fig. 6. 20-hydroxyecdysone reduces NF-κB/p65 stability in bladder cancer. (A-D) T24 and UMUC3 cells were treated with 20-HE (2.5, 5 or 10 μM). After 24 h, all cells were harvested for following assays. (A) RT-qPCR for NF-κB/p65 transcriptional expression calculation in bladder cancer cells. (B) Western blot results for p-NF-κB/p65 and NF-κB/p65 in bladder cancer cells. (C) IF staining for p-NF-κB/p65 and (D) NF-κB/p65 expression levels in T24 and UMUC3 cells. Quantification for p-NF-κB/p65 and NF-κB/p65 fluorescence intensity was exhibited (Scale bar = 15 μm). (E) IHC staining for p-NF-κB/p65 and NF-κB/p65 expression levels in xenograft tumor tissues from each group of mice (Scale bar = 50 μm). Data are displayed as mean ± SD ($n = 3$ or 4 in each group). $^{**}p < 0.01$ $^{***}p < 0.001$ *vs* the Ctrl group.

USP21. As shown in Fig. 7M, we found that USP21 efficiently removed K48-linked polyubiquitination of p65 but not K63-linked ubiquitination. Therefore, USP21 could deubiquitylate K48-linked p65 polyubiquitination, consequently maintaining their stabilization in bladder cancer cells to promote tumor growth. Finally, we found that USP21-mediated K48-linked polyubiquitination of p65 was strongly rescued upon 20-HE coculture in T24 and UMUC3 cells (Fig. 7N), contributing to the degradation of p65.

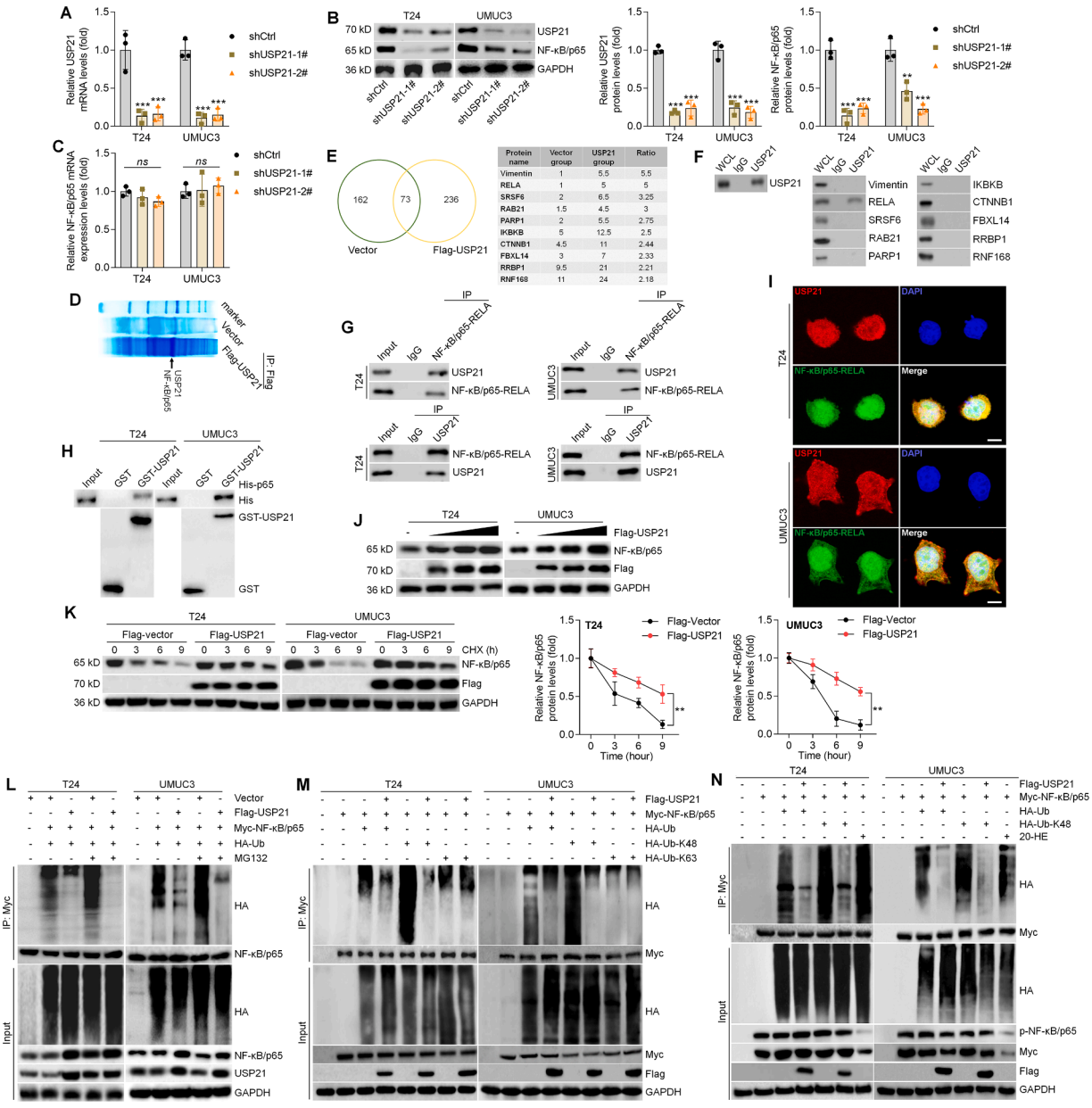

Fig. 7. USP21 directly interacts with p65 and maintains its stability in bladder cancer cells, which can be abrogated by 20-hydroxyecdysone. (A) RT-qPCR analysis of USP21 expression in T24 and UMUC3 cell lines transfected with USP21 shRNAs and shCtrl. (B) Western blotting results for USP21 and NF-κB/p65 in bladder cancer cells with shUSP21 and shCtrl transfection. (C) RT-qPCR analysis of p65 in T24 and UMUC3 cells with USP21 knockdown. (D) Coomassie blue staining on T24 cell line protein samples immunoprecipitated with IgG and anti-USP21 antibody. (E) Identification of USP12 binding partners via a combination of Co-IP and LC-MS/MS analysis. The Venn diagram shows the number of binding partners of USP21 in the two groups. Top ten overlapping proteins with a ratio of >2 were provided. (F) Co-IP assay was performed to explore the interaction between USP21 and the 10 candidates in T24 cells. (G) Immunoblotting to show the interaction between USP21 and p65 in T24 and UMUC3 cells by IP assay. IgG was used as the control. (H) GST pull-down assay was performed to examine the physical interaction between USP21 and p65 in T24 and UMUC3 cells. (I) Double IF staining for USP21 and p65 in T24 and UMUC3 cells. The nuclei were counterstained with DAPI (Scale bar = 15 μm). (J) Western blot analysis of p65 expression in T24 and UMUC3 cells transfected with varying concentrations of Flag-USP21. (K) Western blot analysis of p65 derived from T24 and UMUC3 cells transfected with Flag-USP21 and Flag-empty vector. Cells were incubated with CHX (100 μg/ml) for the shown time. (L) HA-ubiquitin (Ub) was co-expressed with Flag-USP21 in T24 and UMUC3 cells. Western blot analysis was then used to examine the ubiquitination of p65. (M) Western blot analysis for p65 ubiquitination linkage in T24 and UMUC3 cells transfected with Flag-USP21, Myc-p65, and the indicated ubiquitin plasmids. (N) Western blot results for K48-linked p65 ubiquitination in T24 and UMUC3 cells transfected with Flag-USP21, Myc-p65, and the shown ubiquitin plasmids with or without 24 h of 20-HE (10 μM) treatment. Data are displayed as mean ± SD ($n = 3$ in each group). $^{**}p < 0.01$ $^{***}p < 0.001$ *vs* the shCtrl group.

20-hydroxyecdysone-inhibited cell proliferation and EMT process are diminished by USP21

To identify the potential and importance of the USP21 signal in 20-HE-suppressed bladder cancer progression, we then overexpressed USP21 in T24 and UMUC3 cells by transfecting the established plasmids. Overexpression efficiency was confirmed by RT-qPCR and western blot assays (Fig. S4A and B). CCK-8 and EdU staining results showed that promoting USP21 expression markedly enhanced the proliferation of bladder cancer cells, revealing its ontogenetic function in bladder cancer. Of note, we found that the 20-HE-suppressed proliferative ability of T24 and UMUC3 cells was strongly restored when USP21 was

overexpressed (Fig. 8A-C), accompanied by diminished Caspase-3 activity and cleaved expression levels (Fig. 8D and E). We then found that USP21 overexpression not only downregulated the mRNA levels of pro-apoptotic molecule Bax, but also abolished the promotive effects of 20-HE on Bax expression in T24 and UMUC3cells, while opposite results were observed in the expression changes of anti-apoptotic signal Bcl-2 (Fig. S5A). Furthermore, cells transfected with USP21 plasmids exerted stronger migratory and invasive abilities than those of the control group. Importantly, the meliorated cell migration and invasion controlled by 20-HE were markedly regained in bladder cancer cells with USP21 overexpression by transwell analysis (Fig. 8F-H). As expected, 20-HE enhanced expression levels of E-Cadherin were strongly abolished upon USP21 overexpression, while N—Cadherin, Vimentin and MMP13 were significantly restored in 20-HE incubated bladder cancer cells overexpressing USP21 (Fig. S5B). Additionally, western blot analysis was used to calculate NF-κB and p-NF-κB protein expression levels in bladder cancer cells with USP21 overexpression and 20-HE treatment or the two in combination. Immunoblotting results show that promoting USP21 indeed upregulated NF-κB and its phosphorylated protein expression levels in T24 and UMUC3 cells. Notably, 20-HE inhibited NF-κB and p-NF-κB expression levels were strongly restored in bladder cancer cells when USP21 was facilitated (Fig. 8I). These data indicate that the repressive effects of 20-HE on bladder cancer proliferation and the EMT process were partially dependent on USP21/NF-κB signaling suppression. we then treated T24 and UMUC3 cells with shUSP21, followed by 20-HE incubation to further investigate the expression changes of NF-κB activation and its downstream signals associated with apoptosis, migration and invasion. Notably, we found that similar with the inhibitory effects of 20-HE on NF-κB signaling, USP21 knockdown markedly reduced NF-κB and p-NF-κB protein expression levels in bladder cancer cells. Moreover, 20-HE still exerted suppressive influence on the expression of NF-κB and p-NF-κB in T24 and UMUC3 cells with shUSP21 transfection (Supplementary fig. 6A). As expected, USP21 absence significantly reduced the bladder cancer cell proliferative capacity, as indicated by the decreased EdU-positive cells. What's more, 20-HE remained its inhibitory action on the proliferation of bladder cancer cells (Supplementary fig. 6B). Additionally, higher expression levels of cleaved Caspase-3 were detected in T24 and UMUC3 cells with USP21 knockdown, 20-HE exposure or the two in combinational treatments (Supplementary fig. 6C), accompanied with increased Bax gene expression levels and decreased Bcl-2 mRNA levels (Supplementary fig. 7A). Transwell analysis further showed that shUSP21, 20-HE and their combination obviously reduced the migratory and invasive capacity of bladder cancer cells (Supplementary fig. 6D). Meanwhile, NF-κB pathway downstream signals and EMT markers N—Cadherin, Vimentin and MMP13 mRNA expression levels were significantly downregulated in bladder cancer cells with USP21 deletion, 20-HE incubation or their combined administration, whereas E-Cadherin was improved (Supplementary fig. 7B). These data above revealed that USP21 absence could restrain the proliferation, induce apoptosis and inhibit EMT process of bladder cancer cells. Importantly, 20-HE could still perform its anti-cancer role in bladder cancer by mediating these above cellular events when USP21 was knocked down. These results above revealed that USP21 was indeed essential for 20-HE to perform its anti-tumor role in bladder cancer, but possibly not the only signal.

Discussion

Bladder cancer has been recognized as one of the most frequently mutated human cancers with a high incidence and mortality rate, thereby threatening public health. Therapies for bladder cancer consist of surgery, chemotherapy, radiotherapy, and immunotherapy [1-7, 32–34]. Unfortunately, clinical chemoresistance is an unavoidable dilemma for bladder cancer patients with cisplatin or gemcitabine drugs [35]. Herein, we still need to explore the underlying mechanisms and find new efficient drugs to improve the therapeutic outcomes of bladder cancer. Substantial evidence suggests that 20-HE, a natural sterol compound, exerts anti-oxidant, anti-inflammatory, and anti-metabolic disorder properties [19,21,22]. In recent years, its anti-cancer potential has been increasingly focused on [23,24]. However, the influence of 20-HE on human bladder cancer and the underlying mechanism were still in short supply. To the best of our knowledge, this study was the first to report the potential of 20-HE in the treatment of bladder cancer.

In this work, 20-HE was identified as an effective therapeutic approach for bladder cancer treatment in vitro and in vivo. Briefly, 20-HE treatments markedly reduced the proliferation, migration, and invasion of bladder cancer cell lines in a dose-dependent manner. In the established mouse model with bladder cancer, 20-HE significantly reduced tumor growth and limited lung metastasis. Through the RNA sequencing analysis, the potential signals regulated by 20-HE in the suppression of bladder cancer were screened, and USP21 was identified as a promising candidate. Higher USP21 expression was detected in human bladder cancer tissues by using the TCGA database, and a positive correlation between USP21 and p65 (RELA) expression was identified. RT-qPCR and western blot assays confirmed the suppressive effect of 20-HE on USP21 expression in bladder cancer cell lines, which was also proved by in vivo studies. Additionally, p65 mRNA, p65 protein, and its phosphorylation (p-p65) expression levels were also markedly down-regulated by 20-HE in vitro and in vivo, revealing the potential of 20-HE to limit p65 transcription, stability and activation during bladder cancer progression. Mechanistic experiments showed that USP21 could directly interact with p65 and induce its K48-linked deubiquitination, thereby stabilizing the p65 signal in bladder cancer and contributing to tumor growth. Notably, this phenomenon mediated by USP21 was diminished upon 20-HE treatment, resulting in p65 degradation in bladder cancer cells. Moreover, we found that USP21 overexpression significantly abolished the function of 20-HE to restrain the proliferative, migratory, and invasive properties of bladder cancer. Therefore, we assumed that USP21 suppression was necessary for 20-HE to perform its therapeutic role against bladder cancer progression by restricting K48-linked deubiquitination of p65 mediated by USP21. Of note, bladder cancer cells with USP21 knockdown in the absence or presence of 20-HE exerted restrained cell proliferative, migratory and invasive capacities. Combined with the inhibitory of 20-HE on p65 transcription, we concluded that 20-HE could promote NF-κB/p65 protein degradation by its stronger inhibitory effects on USP21, and meanwhile directly inhibit NF-κB/p65 signal from its transcriptional levels, thereby contributing to the suppression of cancer cell proliferation and EMT process and the introduction of apoptosis (Fig. 8J). Together, our results provided evidence that 20-HE might be a promising therapeutic strategy for the treatment of bladder cancer with undetectable toxicity through suppressing USP21/NF-κB signaling pathway.

20-HE is ecdysone substituted by a hydroxyl group at position 20 and has been reported to possess beneficial effects against metabolic disturbance, tissue damage, and tumor growth [19–22]. As reported, 20-HE has anti-proliferative activity in breast cancer cells, partly through inducing apoptosis via the activation of Caspase-3 and down-regulation of the anti-apoptotic signal Bcl-2 [23]. Additionally, 20-HE down-regulates the S-phase entry and presents proapoptotic properties in human lung cancer cells [24]. In line with these studies, we also observed the anti-proliferative and proapoptotic properties of 20-HE in bladder cancer cells in a dose-dependent manner. Caspase-3, as an executioner caspase, plays an imperative role in inducing apoptosis and becomes a promising target for tumor treatment [36]. We also found that Caspase-3 cleavage and activation were strongly triggered by 20-HE in bladder cancer cell lines, while Bcl-2 expression levels were decreased, accompanied by higher apoptotic cell death.

Numerous studies have demonstrated that EMT is a process by which cells lose their epithelial features and go through molecular, biochemical, and/or morphologic alterations, requiring a more undifferentiated and mesenchymal phenotype [37,38]. Furthermore, EMT can confer

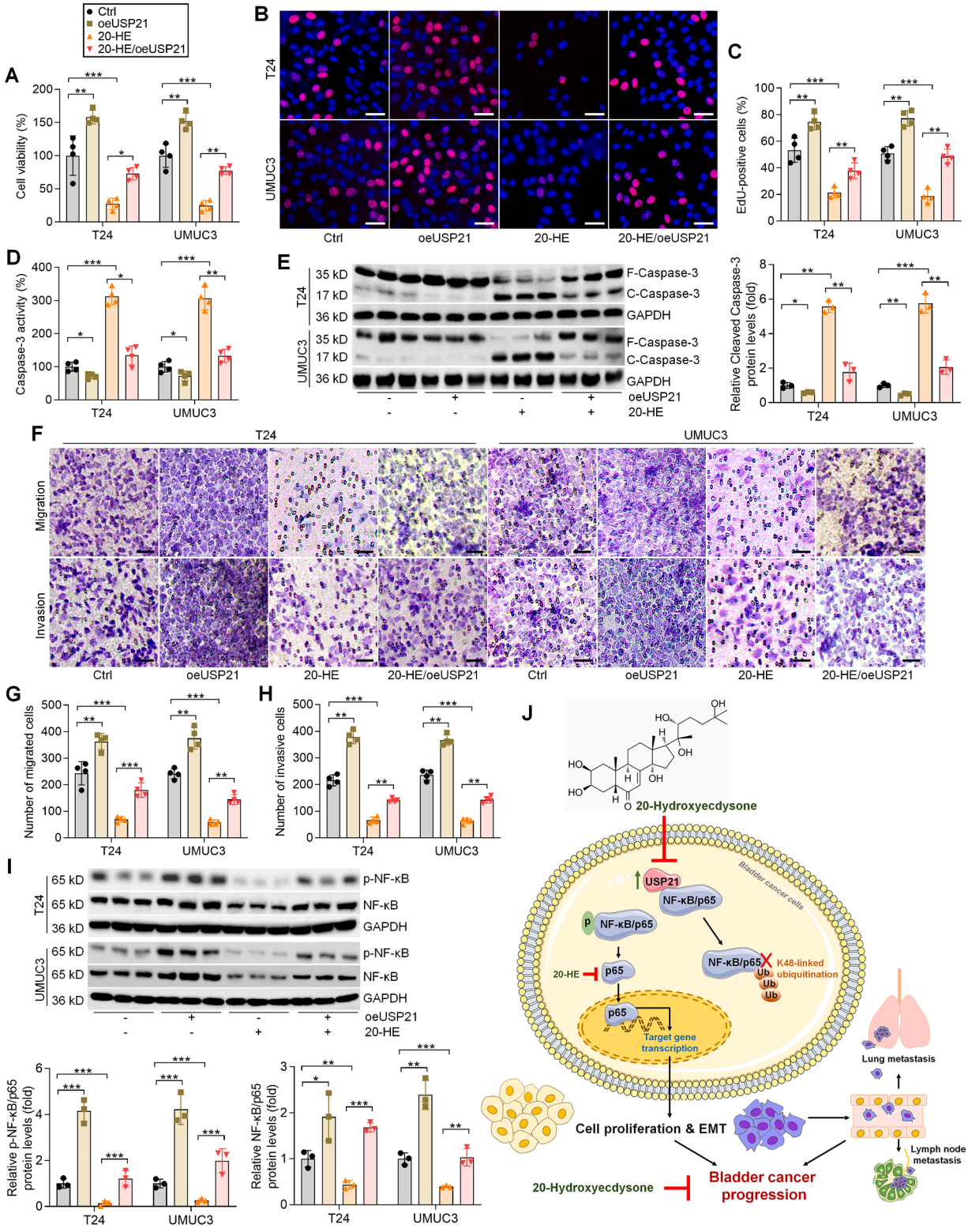

Fig. 8. 20-hydroxyecdysone-inhibited cell proliferation and EMT process are diminished by USP21. (A-I) T24 and UMUC3 cells were transfected with USP21 overexpression plasmids, and were then treated with or without 20-HE (10 μM) for an additional 24 h. Next, all cells were harvested for studies as below. (A) Cell viability was measured using CCK-8 analysis. (B&C) EdU staining was conducted to examine cell proliferation (Scale bar = 50 μm). (D) Caspase-3 activity was assessed. (E) Cleaved Caspase-3 expression levels were measured by western blot analysis. (F) Transwell analysis was performed to examine the migration and invasion of cells (Scale bar = 50 μm). (G) The number of migrated and (H) invasive cells was quantified. (I) Western blot analysis for p-NF-κB/p65 and NF-κB/p65 protein expression levels in bladder cancer cell lines. (J) Working model demonstrating the effects of 20-hydroxyecdysone on bladder cancer progression. In brief, USP21 expression is up-regulated in bladder cancer cells, and can deubiquitinate K48-linked polyubiquitination of p65, thereby maintaining p65 stability. These events contribute to the proliferation and metastasis of bladder cancer. However, 20-HE can strongly restrain USP21 expression levels, and herein destabilize p65; meanwhile, 20-HE can directly inhibit p65 via the transcriptional level, which restrains bladder cancer progression ultimately. Data are displayed as mean ± SD (n = 3 or 4 in each group). *$p < 0.05$, **$p < 0.01$ ***$p < 0.001$.

stem-like properties and cell plasticity, resulting in the acquisition of migratory and invasive phenotypes through impairing cell-cell adhesion, ultimately accelerating metastatic properties or resistance to therapies [39]. EMT has a pivotal role in the metastasis of multiple different types of tumors, including bladder cancer [40]. A previous study indicated that 20-HE appears to exhibit its fibrosis-antagonizing effects by depressing the expression of Snail and restraining EMT processes via improving E-cadherin expression in renal proximal tubules [41]. Here, we also found that the EMT process of bladder cancer cells was strongly inhibited by 20-HE, as proved by the reduced number of cells in migration and invasion status. EMT is frequently activated by a number of EMT-associated transcription factors, such as N-cadherin, vimentin, Twist, slug, and ZEB1/2. Meanwhile, the loss of expression of epithelial markers such as E-cadherin and ZO-1 contributes to EMT [42]. Moreover, MMPs, members of zinc-dependent endopeptidases, are also crucial mediators of tissue reorganization occurring in malignancy. MMP13 is a member of the MMPs family of endopeptidases and participates in invasiveness and metastasis in tumor tissues [43]. In our study, we found that 20-HE could restrain the EMT program in bladder cancer cells, as indicated by the evidently decreased cell migration and invasion, along with increased expression of E-cadherin and ZO-1, but decreased N-cadherin, Vimentin, ZEB1, and MMP13. RNA-Seq analysis also showed that the EMT process was significantly modulated by 20-HE, with several markedly down-regulated genes involved in EMT activation, such as COL1A1, SMAD7, and TGFB1. Results from animal studies confirmed that 20-HE could restrain lung and lymph node metastasis for bladder cancer treatment. Collectively, these results provided further insights into the effect of 20-HE on tumor suppression by weakening EMT and distant organ metastasis.

It has been well known that ubiquitination and associated processes play essential roles in regulating the physiology and pathology of cells, and malfunction of ubiquitylation is involved in a variety of diseases [9]. Thus, dysregulation of DUBs is closely associated with varying diseases, including bladder cancer [44]. Given the crucial role of DUBs in the growth of tumors, pharmacological inhibition of DUBs has been recognized as a potential therapeutic approach for the treatment of cancer. As for this, a growing number of DUB inhibitors have been developed and are presently being tested in preclinical research and clinical trials [45,46]. USP21 is a DUB and belongs to the USP protease family. USP21 is widely overexpressed in multiple different types of tumors, such as breast cancer, pancreatic cancer, lung cancer, and colon cancer [14–16,47]. USP21 has been considered a proliferation and metastasis enhancer during tumor progression. For instance, USP21 contributes to the proliferation, migration, and invasion of NSCLC cells by deubiquitinating Yin Yang-1 (YY1) [47]. Additionally, USP21 could promote colorectal cancer metastasis through its functioning as a Fra-1 deubiquitinase [16]. A previous study initially reported that USP21 is overexpressed in bladder cancer tissues and cell lines and predicts a poor prognosis for bladder cancer. USP21 knockdown weakens the migration and invasion ability of bladder cancer cells and inhibits the EMT process [17]. Here, we confirmed higher expression of USP21 in patients with bladder cancer. More importantly, our RNA sequencing, RT-qPCR, and western blot assays showed that 20-HE markedly reduced the expression of USP21 from mRNA and protein levels in bladder cancer cell lines, which were verified in the dissected tumor tissues from the xenograft mouse model. These data elucidated that 20-HE might act as an inhibitor of USP21 to perform its anti-tumor role in bladder cancer.

The transcription factor NF-κB plays a key role in various cancers and consists of five members, including p65 (RELA), p50 (RELB), c-REL, NF-κB1, and NF-κB2. Accumulating studies have illustrated that NF-κB mainly functions as an oncogene and exerts a quite sophisticated role in tumors [48,49]. The most abundant forms of NF-κB are the p50 and p65 subunits. The subunit of p65 participates in cell survival, proliferation, invasion, metastasis, and angiogenesis [30,31,50]. In brief, constitutively activated NF-κB transcription factors have been associated with several aspects of tumorigenesis, including promoting cancer-cell proliferation, preventing apoptosis, and increasing a tumor's angiogenic and metastatic potential [51,52]. In tumor cells, NF-κB is consequently activated because mutations in genes encoding the NF-κB transcription factors themselves or in genes that control NF-κB activity. Blocking NF-κB can cause tumor cells to stop proliferating, to die, or to become more sensitive to the action of anti-tumor agents [53–55]. In addition to function as an inhibitor of programmed cell death, NF-κB also plays an essential role in mediating migration, invasion and metastasis processes. Cells with elevated NF-κB activity deregulate production of chemokines, which increases migratory activity. Other NF-κB targets contribute to epithelial-mesenchymal transition (vimentin, Twist), remodeling the extracellular matrix through induction of angiogenesis (IL8, VEGF), and promotion of invasion and metastasis (MMP2, MMP9) [56–59]. Thus, targeting genes induced by NF-κB activation, or inactivation of the NF-κB pathway, could serve as therapeutic targets for treatment of bladder cancer. Posttranslational regulation of NF-κB/p65 provides critical mechanisms to differentially mediate the activation of NF-κB signaling in a mass of types of tumors [60,61]. Methods to lower p65 expression or activation have been proven to be effective for tumor treatment [62]. Emerging studies demonstrate that the ubiquitination of p65 is important for mediating its function [31,61]. The main deliverables for protein ubiquitination modulation are the linkages of many ubiquitin chains with the protein substrates. Among these varying ubiquitin chains, K63- and 48-linked chains are recognized as the most common types [63]. Accordingly, K63-linked chains target proteins for ubiquitination to regulate the activity of the protein, while K48-linked chains target proteins for proteasome-regulated degradation [64]. Inhibitor of Growth 4 (ING4) performs as an E3 ubiquitin ligase to induce K48-linked ubiquitination of p65 and thus its degradation, contributing to the termination of NF-κB activation [65]. In addition, peroxisome proliferator-activated receptor gamma (PPARγ), also as an E3 ubiquitin ligase, could interact with p65 and suppress NF-κB activation by triggering its proteasome-dependent degradation [66]. A previous study claimed that USP21 could affect the transcription of NF-κB/p65 through deubiquitination [67]. In our present study, we observed a positive correlation between USP21 and p65 expression levels in bladder cancer patients. Besides USP21 down-regulation, we also found a significant reduction of p65 in 20-HE-treated bladder cancer cells by RNA sequencing analysis. RT-qPCR and western blot analysis confirmed that 20-HE treatments dose-dependently reduced p65 mRNA, phosphorylation and stability in bladder cancer cells, which were confirmed by IF and IHC staining in vitro and in vivo, respectively. These data suggested that 20-HE might directly inhibit p65 transcriptional expression levels and meanwhile induce its protein degradation to restrain bladder cancer onsetting, herein leading to the suppression of its down-stream signals involved in EMT and induction of cell apoptosis. Mechanistic studies further showed that USP21 acted as a DUB, deubiquitinating p65 at K48 and thus removing its degradation and maintaining its stability in bladder cancer cells, thereby contributing to p65 activation and bladder cancer development. Intriguingly, 20-HE interference obviously restored K48-linked p65 ubiquitination induced by USP21 in bladder cancer cells, resulting in p65 degradation and phosphorylation inhibition, which might be attributed to the inhibitory effect of 20-HE on USP21. Importantly, promoting USP21 could markedly enhance the proliferation, migration, and invasion of bladder cancer cells and considerably abolish the anti-proliferative and anti-migratory functions of 20-HE, along with restored NF-κB/p65 and its phosphorylation expression levels. These results elucidated that USP21 suppression was at least in part associated with the inhibitory effects of 20-HE on bladder cancer progression. Moreover, in bladder cancer cells with USP21 knockdown, 20-HE could still perform its function to restrain the cell proliferative, migratory and invasive capacities with reduced NF-κB/p65 and p-NF-κB/p65 expression levels, revealing that USP21 expression suppression might be not the only way for 20-HE during bladder cancer inhibition.

In conclusion, we provided new insights into the roles of USP21 in

bladder cancer. USP21 was a p65 DUB that removed K48-linked ubiquitination of p65 and suppressed its degradation, contributing to bladder cancer cell growth, the EMT program, and metastasis via its deubiquitylation activity. 20-HE on the one could directly suppress NF-κB/p65 signaling from transcriptional levels, and on the other could function as an inhibitor of USP21 to induce p65 protein degradation and its activation blockage, thereby prohibiting bladder cancer progression (Fig. 8J). Our findings not only identify new targets of 20-HE but also provide solid evidence for its clinical application in bladder cancer treatment in the future, which deserves further validation to ensure its safety and effectiveness for human patients.

CRediT authorship contribution statement

Qiang Ma: Conceptualization, Data curation, Formal analysis, Methodology, Project administration, Resources, Software, Supervision, Validation, Visualization, Writing – original draft, Funding acquisition, Writing – review & editing. **Fei Wu:** Conceptualization, Data curation, Formal analysis, Methodology, Project administration, Resources, Software, Supervision, Validation, Visualization, Writing – original draft, Funding acquisition, Writing – review & editing. **Xiaohui Liu:** Conceptualization, Data curation, Formal analysis, Supervision, Validation, Visualization, Writing – original draft. **Cuifang Zhao:** Conceptualization, Data curation, Formal analysis, Supervision, Validation, Visualization, Writing – original draft. **Yang Sun:** Conceptualization, Data curation, Formal analysis. **Yuanyuan Li:** Conceptualization, Data curation, Formal analysis. **Wei Zhang:** Conceptualization, Data curation, Formal analysis, Funding acquisition, Writing – review & editing. **Hongge Ju:** Conceptualization, Data curation, Formal analysis, Methodology, Project administration, Resources, Software, Supervision, Validation, Visualization, Writing – original draft, Funding acquisition, Writing – review & editing. **Yukun Wang:** Writing – original draft, Project administration, Methodology, Investigation, Funding acquisition, Formal analysis, Data curation, Conceptualization.

Declaration of competing interest

The authors see no competing interests.

Acknowledgment

This work was supported by the Natural Science Foundation of Inner Mongolia Autonomous Region of China (No. 2017BS0805 and 2021MS08009), the Program for Young Talents of Science and Technology in Universities of Inner Mongolia Autonomous Region (No. NJYT-20-B22), Shenzhen University Stability Support Program (No. 20200925160201001), General Project of Southern University of Science and Technology Hospital (No.2020-A2) and the Nanshan and District (Shenzhen) Education (Health) Science and Technology Project (No. 2020009).

Supplementary materials

Supplementary material associated with this article can be found, in the online version, at doi:10.1016/j.tranon.2024.101958.

References

[1] K. Saginala, A. Barsouk, J.S. Aluru, et al., Epidemiology of bladder cancer, Med. Sci. 8 (1) (2020) 15.
[2] A. Jung, M.E. Nielsen, J.L. Crandell, et al., Quality of life in non-muscle-invasive bladder cancer survivors: a systematic review, Cancer Nurs. 42 (3) (2019) E21–E33.
[3] L. Tran, J.F. Xiao, N. Agarwal, et al., Advances in bladder cancer biology and therapy, Nat. Rev. Cancer 21 (2) (2021) 104–121.
[4] X. Chen, J. Zhang, W. Ruan, et al., Urine DNA methylation assay enables early detection and recurrence monitoring for bladder cancer, J. Clin. Invest. 130 (12) (2020) 6278–6289.
[5] A. Schulz, J. Loloi, L. Pina Martina, et al., The development of non-invasive diagnostic tools in bladder cancer, Onco Targets. Ther. (2022) 497–507.
[6] R. Nadal, J. Bellmunt, Management of metastatic bladder cancer, Cancer Treat. Rev. 76 (2019) 10–21.
[7] A. Lopez-Beltran, A. Cimadamore, A. Blanca, et al., Immune checkpoint inhibitors for the treatment of bladder cancer, Cancers. (Basel) 13 (1) (2021) 131.
[8] J.J. Meeks, H. Al-Ahmadie, B.M. Faltas, et al., Genomic heterogeneity in bladder cancer: challenges and possible solutions to improve outcomes, Nat. Rev. Urol. 17 (5) (2020) 259–270.
[9] L. Deng, T. Meng, L. Chen, et al., The role of ubiquitination in tumorigenesis and targeted drug discovery, Signal. Transduct. Target. Ther. 5 (1) (2020) 11.
[10] F. Trulsson, V. Akimov, M. Robu, et al., Deubiquitinating enzymes and the proteasome regulate preferential sets of ubiquitin substrates, Nat. Commun. 13 (1) (2022) 2736.
[11] T. Yuan, Z. Chen, F. Yan, et al., Deubiquitinating enzyme USP10 promotes hepatocellular carcinoma metastasis through deubiquitinating and stabilizing Smad4 protein, Mol. Oncol. 14 (1) (2020) 197–210.
[12] T. An, Y. Lu, X. Yan, et al., Insights into the properties, biological functions, and regulation of USP21, Front. Pharmacol. 13 (2022) 944089.
[13] A. Kim, J.H. Koo, X. Jin, et al., Ablation of USP21 in skeletal muscle promotes oxidative fibre phenotype, inhibiting obesity and type 2 diabetes, J. Cachexia, Sarcopenia Muscle 12 (6) (2021) 1669–1689.
[14] P. Hou, X. Ma, Q. Zhang, et al., USP21 deubiquitinase promotes pancreas cancer cell stemness via Wnt pathway activation, Genes Dev. 33 (19–20) (2019) 1361–1366.
[15] A. Arceci, T. Bonacci, X. Wang, et al., FOXM1 deubiquitination by USP21 regulates cell cycle progression and paclitaxel sensitivity in basal-like breast cancer, Cell Rep. 26 (11) (2019) 3076–3086, e6.
[16] S.I. Yun, H.K. Hong, S.Y. Yeo, et al., Ubiquitin-specific protease 21 promotes colorectal cancer metastasis by acting as a Fra-1 deubiquitinase, Cancers (Basel) 12 (1) (2020) 207.
[17] Y. Chen, B. Zhou, D. Chen, USP21 promotes cell proliferation and metastasis through suppressing EZH2 ubiquitination in bladder carcinoma, Onco Targets. Ther. (2017) 681–689.
[18] S.Y. Jeon, K.A. Hwang, K.C. Choi, Effect of steroid hormones, estrogen and progesterone, on epithelial mesenchymal transition in ovarian cancer development, J. Steroid Biochem. Mol. Biol. 158 (2016) 1–8.
[19] L. Dinan, W. Dioh, S. Veillet, et al., 20-Hydroxyecdysone, from plant extracts to clinical use: therapeutic potential for the treatment of neuromuscular, cardio-metabolic and respiratory diseases, Biomedicines. 9 (5) (2021) 492.
[20] X.F. Zhao, G protein-coupled receptors function as cell membrane receptors for the steroid hormone 20-hydroxyecdysone, Cell Commun. Signal. 18 (1) (2020) 146.
[21] J. Buniam, P. Chansela, J. Weerachayaphorn, et al., Dietary supplementation with 20-hydroxyecdysone ameliorates hepatic steatosis and reduces white adipose tissue mass in ovariectomized rats fed a high-fat, high-fructose diet, Biomedicines 11 (7) (2023) 2071.
[22] Y. Sun, D.L. Zhao, Z.X. Liu, et al., Beneficial effect of 20hydroxyecdysone exerted by modulating antioxidants and inflammatory cytokine levels in collageninduced arthritis: a model for rheumatoid arthritis, Mol. Med. Rep. 16 (5) (2017) 6162–6169.
[23] A. Romaniuk-Drapała, N. Lisiak, E. Totoń, et al., Proapoptotic and proautophagic activity of 20-hydroxyecdysone in breast cancer cells in vitro, Chem. Biol. Interact. 342 (2021) 109479.
[24] O. Shuvalov, Y. Kirdeeva, E. Fefilova, et al., 20-Hydroxyecdysone confers antioxidant and antineoplastic properties in human non-small cell lung cancer cells, Metabolites. 13 (5) (2023) 656.
[25] H. Pimentel, N.L. Bray, S. Puente, et al., Differential analysis of RNA-seq incorporating quantification uncertainty, Nat. Methods 14 (7) (2017) 687–690.
[26] F. Zhang, C.K. Deng, M. Wang, et al., Identification of novel alternative splicing biomarkers for breast cancer with LC/MS/MS and RNA-Seq, BMC Bioinform.. 21 (2020) 1–17.
[27] J. Tang, S. Tu, G. Lin, et al., Sequential ubiquitination of NLRP3 by RNF125 and Cbl-b limits inflammasome activation and endotoxemia, J. Exp. Med. 217 (4) (2020) e20182091.
[28] Mao Y., Peng X., Xue P., et al. Network pharmacology study on the pharmacological mechanism of cinobufotalin injection against lung cancer. Evidence-Based Complementary and Alternative Medicine, 2020, 2020.
[29] Y. Jin, D.T.N. Huynh, T.L.L. Nguyen, et al., Therapeutic effects of ginsenosides on breast cancer growth and metastasis, Arch. Pharm. Res. 43 (2020) 773–787.
[30] Z. Zou, B. Huang, X. Wu, et al., Brd4 maintains constitutively active NF-κB in cancer cells by binding to acetylated RelA, Oncogene 33 (18) (2014) 2395–2404.
[31] M. Cong, Y. Wang, Y. Yang, et al., MTSS1 suppresses mammary tumor-initiating cells by enhancing RBCK1-mediated p65 ubiquitination, Nat. Cancer 1 (2) (2020) 222–234.
[32] Q. Zhang, S. Liu, H. Wang, et al., ETV4 mediated tumor-associated neutrophil infiltration facilitates lymphangiogenesis and lymphatic metastasis of bladder cancer, Adv. Sci. 10 (11) (2023) 2205613.
[33] M. Huang, W. Dong, R. Xie, et al., HSF1 facilitates the multistep process of lymphatic metastasis in bladder cancer via a novel PRMT5-WDR5-Dependent transcriptional program, Cancer Commun. 42 (5) (2022) 447–470.
[34] R. Xie, L. Cheng, M. Huang, et al., NAT10 drives cisplatin chemoresistance by enhancing ac4C-associated DNA repair in bladder cancer, Cancer Res. 83 (10) (2023) 1666–1683.
[35] J. Pan, X.U. Li, W. Wu, et al., Long non-coding RNA UCA1 promotes cisplatin/gemcitabine resistance through CREB modulating miR-196a-5p in bladder cancer cells, Cancer Lett. 382 (1) (2016) 64–76.

[36] P. Yadav, R. Yadav, S. Jain, et al., Caspase-3: a primary target for natural and synthetic compounds for cancer therapy, Chem. Biol. Drug Des. 98 (1) (2021) 144–165.
[37] T. Brabletz, R. Kalluri, M.A. Nieto, et al., EMT in cancer, Nat. Rev. Cancer 18 (2) (2018) 128–134.
[38] M. Saitoh, Involvement of partial EMT in cancer progression, J. Biochem. 164 (4) (2018) 257–264.
[39] Y. Huang, W. Hong, X. Wei, The molecular mechanisms and therapeutic strategies of EMT in tumor progression and metastasis, J. Hematol. Oncol. 15 (1) (2022) 129.
[40] S.S. Islam, R.B. Mokhtari, A.S. Noman, et al., Sonic hedgehog (Shh) signaling promotes tumorigenicity and stemness via activation of epithelial-to-mesenchymal transition (EMT) in bladder cancer, Mol. Carcinog. 55 (5) (2016) 537–551.
[41] T.J. Hung, W.M. Chen, S.F. Liu, et al., 20-Hydroxyecdysone attenuates TGF-β1-induced renal cellular fibrosis in proximal tubule cells, J. Diabetes Complicat. 26 (6) (2012) 463–469.
[42] Odero-Marah V., Hawsawi O., Henderson V., et al. Epithelial-mesenchymal transition (EMT) and prostate cancer. Cell & molecular biology of prostate cancer: updates, insights and new frontiers, 2018: 101–110.
[43] G.H. Shi, Y.F. Cheng, Y. Zhang, et al., Long non-coding RNA LINC00511/miR-150/MMP13 axis promotes breast cancer proliferation, migration and invasion, Biochim. Biophys. Acta (BBA)-Mol. Basis Dis. 1867 (3) (2021) 165957.
[44] M. Wang, Z. Zhang, Z. Li, et al., E3 ubiquitin ligases and deubiquitinases in bladder cancer tumorigenesis and implications for immunotherapies, Front. Immunol. (2023) 14.
[45] P. Farshi, R.R. Deshmukh, J.O. Nwankwo, et al., Deubiquitinases (DUBs) and DUB inhibitors: a patent review, Expert. Opin. Ther. Pat. 25 (10) (2015) 1191–1208.
[46] J.M. Fraile, V. Quesada, D. Rodríguez, et al., Deubiquitinases in cancer: new functions and therapeutic options, Oncogene 31 (19) (2012) 2373–2388.
[47] P. Xu, H. Xiao, Q. Yang, et al., The USP21/YY1/SNHG16 axis contributes to tumor proliferation, migration, and invasion of non-small-cell lung cancer, Exp. Mol. Med. 52 (1) (2020) 41–55.
[48] G. Maubach, M.H. Feige, M.C.C. Lim, et al., NF-kappaB-inducing kinase in cancer, Biochim. Biophys. Acta (BBA)-Rev. Cancer 1871 (1) (2019) 40–49.
[49] F.H. Sarkar, Y. Li, NF-kappaB: a potential target for cancer chemoprevention and therapy, Front. Biosci. 13 (1) (2008) 2950–2959.
[50] W. Weichert, M. Boehm, V. Gekeler, et al., High expression of RelA/p65 is associated with activation of nuclear factor-κB-dependent signaling in pancreatic cancer and marks a patient population with poor prognosis, Br. J. Cancer 97 (4) (2007) 523–530.
[51] S. Prasad, J. Ravindran, B.B. Aggarwal, NF-κB and cancer: how intimate is this relationship, Mol. Cell. Biochem. 336 (2010) 25–37.
[52] R.O. Escarcega, S. Fuentes-Alexandro, M. Garcia-Carrasco, et al., The transcription factor nuclear factor-kappa B and cancer, Clin. Oncol. 19 (2) (2007) 154–161.
[53] X. Cui, D. Shen, C. Kong, et al., NF-κB suppresses apoptosis and promotes bladder cancer cell proliferation by upregulating survivin expression in vitro and in vivo, Sci. Rep. 7 (1) (2017) 40723.
[54] S.T. Tan, S.Y. Liu, B. Wu, TRIM29 overexpression promotes proliferation and survival of bladder cancer cells through NF-κB signaling, Cancer Res. Treat. 48 (4) (2016) 1302, official journal of Korean Cancer Association.
[55] E.C. Merkhofer, P. Cogswell, A.S. Baldwin, Her2 activates NF-κB and induces invasion through the canonical pathway involving IKKα, Oncogene 29 (8) (2010) 1238–1248.
[56] C.M. Overall, C. López-Otín, Strategies for MMP inhibition in cancer: innovations for the post-trial era, Nat. Rev. Cancer 2 (9) (2002) 657–672.
[57] M.A. Huber, N. Azoitei, B. Baumann, et al., NF-κB is essential for epithelial-mesenchymal transition and metastasis in a model of breast cancer progression, J. Clin. Invest. 114 (4) (2004) 569–581.
[58] Q. Wu, X. Zhou, P. Li, et al., ROC1 promotes the malignant progression of bladder cancer by regulating p-IκBα/NF-κB signaling, J. Exp. Clin. Cancer Res. 40 (1) (2021) 158.
[59] J. Girouard, D. Belgorosky, J. Hamelin-Morrissette, et al., Molecular therapy with derivatives of amino benzoic acid inhibits tumor growth and metastasis in murine models of bladder cancer through inhibition of TNFα/NFKB and iNOS/NO pathways, Biochem. Pharmacol. 176 (2020) 113778.
[60] K. Taniguchi, M. Karin, NF-κB, inflammation, immunity and cancer: coming of age, Nat. Rev. Immunol. 18 (5) (2018) 309–324.
[61] J. Jin, Z. Lu, X. Wang, et al., E3 ubiquitin ligase TRIM7 negatively regulates NF-kappa B signaling pathway by degrading p65 in lung cancer, Cell. Signal. 69 (2020) 109543.
[62] X. Pan, T. Arumugam, T. Yamamoto, et al., Nuclear factor-κB p65/relA silencing induces apoptosis and increases gemcitabine effectiveness in a subset of pancreatic cancer cells, Clin. Cancer Res. 14 (24) (2008) 8143–8151.
[63] I.E. Wertz, V.M. Dixit, Regulation of death receptor signaling by the ubiquitin system, Cell Death Differ. 17 (1) (2010) 14–24.
[64] J.J. Sims, R.E. Cohen, Linkage-specific avidity defines the lysine 63-linked polyubiquitin-binding preference of rap80, Mol. Cell 33 (6) (2009) 775–783.
[65] Y. Hou, Z. Zhang, Q. Xu, et al., Inhibitor of growth 4 induces NFκB/p65 ubiquitin-dependent degradation, Oncogene 33 (15) (2014) 1997–2003.
[66] Y. Hou, F. Moreau, K. Chadee, PPARγ is an E3 ligase that induces the degradation of NFκB/p65, Nat. Commun. 3 (1) (2012) 1300.
[67] L. Tao, C. Chen, H. Song, et al., Deubiquitination and stabilization of IL-33 by USP21, Int. J. Clin. Exp. Pathol. 7 (8) (2014) 4930.